Battery Management System

for the Wireless Powerlizer

J.C. van Ammers
H. Chen

Bachelor Thesis

June 30, 2021

TU Delft

Battery Management System

for the Wireless Powerlizer

by

J.C. van Ammers
H. Chen

to obtain the degree of Bachelor of Science
at the Delft University of Technology.

Authors:	J.C. van Ammers	4818369
	H. Chen	4961293
Project duration:	April 19, 2021 – July 2, 2021	
Supervisors:	Dr. J. Dong,	
	C. Riekerk.	
Thesis committee:	Dr.ing. I.E. Lager,	TU Delft
	Dr. J. Dong,	TU Delft
	Dr. T.B. Soeiro.	TU Delft

An electronic version of this thesis is available at http://repository.tudelft.nl/.

TU Delft

Abstract

To enable the portable use of electronic devices, (rechargeable) batteries need to be used. These batteries require a battery management system in order for them to operate safely and efficiently. This thesis describes such a system for the Wireless Powerlizer: a power bank with wireless charging capabilities and an integrated sterilizer using UV-C light.

The battery management system comprises of a charging circuit, a protection module, and cell balancing features. These features are designed to function with Li-ion batteries, which are chosen for their high volumetric energy density, in a 5S1P configuration. These batteries will be charged via a constant-current, constant-voltage (CC-CV) scheme in order to improve charging speed. This charging scheme will be facilitated by a DC-DC boost converter with current and voltage control.

The mechanism behind the protection module (overcharge, overdischarge, overcurrent, and temperature) and passive cell balancing features are elucidated via flowcharts and also verified by simulation in Simulink. A prototype encompassing the charging circuit is implemented on a PCB and tested. The realized boost converter successfully allows for CC-CV charging: it operates at 263 kHz, has a charging current of 1 A, a constant voltage boundary of 19.6 V, and shows an efficiency of 92–93.6 %.

Preface

This thesis was written as part of the Bachelor Graduation Project at the Delft University of Technology. The project was divided into three subgroups, each with two students. The battery management system of the Wireless Powerlizer is treated in this thesis. The project duration was 9 weeks. During this time a literature study was performed, a design has been created, and a prototype has been built. In those weeks, a lot has been learned.

This project could not have been completed without the help of our supervisors: Jianning Dong and Thiago Batista Soeiro. We also want to sincerely thank our daily supervisor Calvin Riekerk, who helped us significantly with troubleshooting and ensuring we keep up with the required pace. Furthermore, we extend our thanks to the supervisors of the other subgroups of this project: Guangyao Yu and Wenli Shi. A special thanks is given to the technicians of the DCE&S Group: Bart Roodenburg, Harrie Olsthoorn, and Joris Koeners for helping us with assembling, soldering, and testing the prototype PCB. Lastly, we of course want to express our gratitude to the members of the other subgroups: Charlotte De Jonghe, Gijs Lagerweij, Brecht Hurkmans, and Floris van der Kolk, without whom this project would not have been possible.

J.C. van Ammers
H. Chen
Delft, June 2021

Contents

1 Introduction

The current COVID-19 pandemic has increased the demand for the disinfection of personal belongings. Mobile phones, for example, are frequently touched and thus facilitate the spreading of viruses and bacteria, and thus should be disinfected often. Furthermore, these phones run on batteries meaning that they need to be recharged relatively frequently. An increasing amount of phone manufacturers implement wireless charging features. Power banks can be a helpful tool for recharging batteries, with the added convenience of being portable and small. A product that combines both sterilization and charging increases ease of use, and reduces the total time needed for sterilization and charging, by performing them simultaneously.

1.1. Project objective

This project will focus on designing the Wireless Powerlizer: a power bank and sterilizer as one product. The power bank should run on batteries, be chargeable via a USB-C connection, support wireless charging, and the sterilizer should disinfect personal belongings with UV-C light. The project is split into three parts: battery management system, wireless charging, and UV-C sterilization. The top-level project overview is depicted in Figure 1.1.

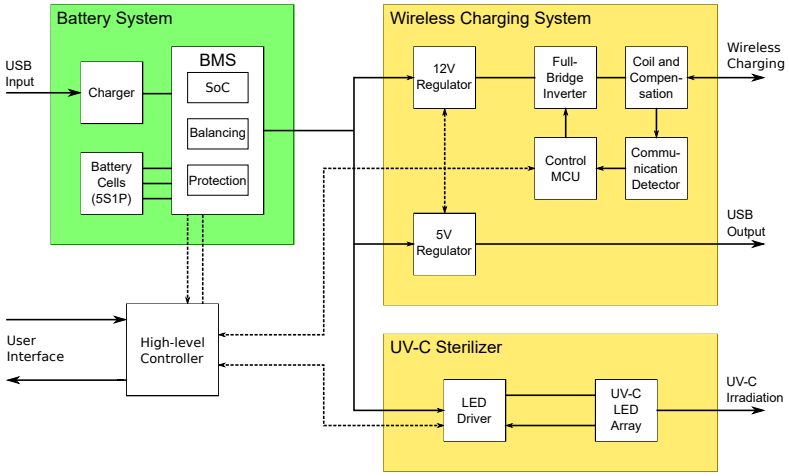

Figure 1.1: The general overview of the different subparts of the total project.

A 3D model of the Wireless Powerlizer is shown in Figure 1.2. All circuit boards integrated in the model were made as part of the prototype. From left to right, the wireless charging PCB, the coil, the sterilizer PCB, the battery management system PCB, and the battery pack can be seen. Furthermore, the Powerlizer has an adjustable lid that is used to close and open the device.

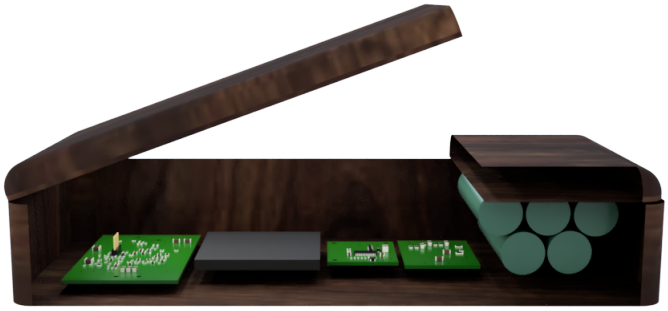

Figure 1.2: 3D Model of the Wireless Powerlizer.

This thesis focuses on the battery management system. Since batteries can severely damage their environment if left uncontrolled, the battery management system should prevent this. It should also be optimized for fast charging of the battery and supply the rest of the Powerlizer with sufficient energy and power. The design of the UV-C sterilizer and wireless charging system is done in other theses [1, 2].

1.2. Analysis

Rechargeable battery cells have existed for several decades. The first rechargeable battery cell was invented by Gaston Plante in 1859 [3]. This battery was based on a lead-acid chemistry and set the basis for new technological progress. Since then, the limits of the lead-acid battery chemistry were discovered. Newer battery cells have been invented which are smaller in size and have higher energy densities.

A battery management system is used to enhance battery lifetime and make optimal use of the capacity available. It controls the currents going in and out of the battery. Charging and discharging a battery needs to be done in such a manner that the battery will not be damaged [4]. Portable electronic devices have experienced rapid growth over the last several decades. This growth goes together with the battery technology development. Despite several improvements of the battery management system that have been made during the last decades, the limiting factor in the technological advancement of portable electronic devices still is the battery system [5].

Since portable devices are developing more rapidly than battery systems, the demands that battery management systems have to meet are very high. This thesis will focus on the design of a battery management system for the Wireless Powerlizer. It shall follow last decades developments, such as smaller size, higher capacity, faster charging, and lower costs.

1.3. Thesis outline

This thesis is divided into several parts. First, in Chapter 2, the program of requirements is outlined. Chapter 3 explains the battery cell. The cell chemistry is selected together with a suitable topology such that the requirements can be met. In Chapter 4, the charging method for the battery is selected. First, a controller is chosen for the USB-C input. After that, the preferred charging method for the battery cells is selected. Based on this, a DC/DC converter is designed with the subsequent control circuit. Finally, the converter is verified by simulations. In Chapter 5, the battery management for safe operation is discussed. The battery management algorithm is elucidated with flowcharts and finally verified by simulations.

A prototype for the charging circuit is designed using KiCad in Chapter 6. The prototype has been verified by tests. Conclusions and recommendations are given in Chapter 7. Appendix A shows the abbreviations used in this thesis.

2

Program of Requirements

This chapter describes the program of requirements as given by the project outline and set by the team. The requirements are separated into Powerlizer requirements and battery management system requirements.

2.1. Powerlizer requirements

The requirements for the entire Wireless Powerlizer system are derived from the project objective and can be divided into several categories. The functional requirements specify what functionality the system must provide.

[**SF.1**] The Powerlizer shall be able to provide two full (0–100 %) wireless phone charges to a phone with average battery capacity (roughly 3500 mAh). This will determine the minimum required battery capacity, as well as the wireless charging time.

[**SF.2**] The Powerlizer shall have a USB-C port for charging the internal battery. An official USB protocol shall be supported.

[**SF.3**] The Powerlizer shall be able to disinfect an area of 10 cm × 17.5 cm. These dimensions are chosen such that most modern smartphones will fit in the disinfection area. Modern smartphone dimensions typically range between 65–80 mm width, 145–170 mm height, and 7.5–10 mm thickness.

- [**SF.3.1**] The disinfection should inactivate the most common microbes found on mobile phones.
- [**SF.3.2**] The disinfection should inactivate at least 99 % and preferably even 99.9 % of these microbes. This corresponds to a 2 or 3 log reduction, respectively.

[**SF.4**] The state of charge of the power bank shall be displayed on an LED indicator. These LEDs may also be used for other user interface purposes (such as displaying disinfection status, wireless charging status, etc.)

Taking into account the portable nature of the Wireless Powerlizer, the allowable operating conditions, aspects of the enclosure, and product dimensions must be considered.

[**SO.1**] The Powerlizer shall be able to operate in ambient temperatures between 0–45 °C. The allowable temperature range is limited by the operating temperature of the battery cells.

[**SO.2**] The Powerlizer enclosure shall be

- [**SO.2.1**] Capable of withstanding temperatures up to 60 °C.
- [**SO.2.2**] Splash resistant.

[**SO.3**] The Powerlizer enclosure shall be at most 12.5 cm × 27.5 cm × 6 cm.

Safety is another important aspect since the Powerlizer will be used in close proximity to humans.

[**SS.1**] The Powerlizer shall follow the relevant IEC, ISO, and national safety regulations.

[**SS.2**] The disinfection area shall not be accessible while the disinfection LEDs are turned on. If the area is opened, disinfection must stop as soon as possible.

[**SS.3**] The wireless charging system must comply with EMI, electromagnetic field exposure, and safety regulations.

2.2. Battery management system requirements

The battery management system has some functional requirements which it shall meet.

[**F.1**] The battery shall be chargeable via USB-C connection. The profile shall be support the official USB protocol.

[**F.2**] The battery shall be able to deliver at least 34 W.

- [**F.2.1**] The Wireless Charging module requires 30 W [2] (considering 50 % efficiency) .
- [**F.2.2**] The Sterilizer module requires 4 W [1].

[**F.3**] The battery shall be able to provide at least two full (0–100 %) phone charges to a phone with average battery capacity (roughly 3500 mAh).

- [**F.3.1**] The battery voltage shall be at least 15 V as specified by the wireless charging module [2].
- [**F.3.2**] The charging efficiency is 50 % as specified by the wireless charging module. [2]

[**F.4**] The battery shall be able to provide at least enough energy to disinfect an area of 10cm×17.5cm. This requires 1.5 Wh [1].

[**F.5**] The battery shall be able to deliver at least enough energy for the controllers.

- [**F.5.1**] Each of 3 modules use a maximum of one micro-controller.
- [**F.5.2**] The micro-controllers each require a maximum of 500 µA over a potential of 3.3 V.
- [**F.5.3**] The controllers shall be supplied as long as the battery is not empty.

[**F.6**] The state of charge of the battery shall be displayed on an LED indicator. These LEDs may also be used for other user interface purposes (such as displaying disinfection status, wireless charging status, etc).

Safety is an important aspect. The battery management system shall meet the safety requirements.

[**S.1**] The system should follow the relevant safety measures mentioned in technical standard IEC 62113:2017.

The trade-off requirements are given as follows.

[**T.1**] The battery weight should be minimized.

[**T.2**] The battery costs should be minimized.

[**T.3**] Switching frequencies in the range of 80–200 kHz should be avoided to minimize interference with the wireless charger.

[**T.4**] The battery capacity should be maximized.

[**T.5**] The battery should support charging as fast as possible.

3

Battery Cell

In this chapter, the battery type and its topology are selected. First, different battery chemistries are discussed and compared. Based on their properties, the battery cell type is chosen. Then, the topology of cells forming a battery is presented. Finally, the battery is selected based on commercially available cells.

3.1. Battery chemistry

A battery cell consists of three main parts: a positive electrode, a negative electrode, and an electrolyte in between. During discharging, an oxidation reaction is initiated between the electrolyte and negative electrode (anode) forming an excess of electrons. The electrolyte allows electrons to flow to the positive electrode (cathode) through a connected load. Here, a reduction reaction takes place. This process is reversed during battery charging. The negative electrode becomes the cathode and the positive electrode the anode.

The battery capacity is expressed in the units of Ah. The C-rate defines the current to charge or discharge a battery and is expressed as the ratio of the current relative to the battery capacity [6]. When a battery is charged to a higher potential than specified, the battery is overcharged and this could cause thermal runaway: increasing temperature initiates exothermic chemical reactions and causes the temperature to rise further. Batteries could catch fire under these conditions [6–8].

There are many widely-known battery chemistry types where lead-acid, nickel-based, and lithium-ion are the most widely used in commercial consumer devices. The chemical reactions for charging and discharging these battery types are shown in Appendix B.1.

3.1.1. Lead-acid

Lead-acid (Pb-acid) is an old widely used rechargeable battery chemistry with the negative electrode made of Lead (Pb), the positive electrode coated with lead-oxide ($PbSO_2$), and the electrolyte containing sulfuric acid (H_2SO_4) and water (H_2O) [9]. The practical energy density of lead-acid batteries is approximately 35 Wh/kg and its nominal cell voltage is 2 V [6, 9, 10].

Lead-acid batteries do not support very fast charging and are limited to 0.25C [10]. They do support very high burst C-rating discharging [11] but have a relative low sustained discharging rate. Their charge-discharge efficiency lies between 50–85 % [12]. Additionally, they have low self-discharge rates (less than 5 % per month). Lead-acid batteries have a relatively high overcharge tolerance, and can operate in a wide temperature range: from −20 °C to 60 °C. While its electrical properties are more stable than other battery types, chemically the electrolyte is very toxic. On top of this, while overcharging does not harm the battery much, it does generate hydrogen and oxygen gases due to electrolysis which need to be removed by ventilation to reduce the risk of explosions [11]. Furthermore, lead-acid batteries do have a low initial cost (€125 to €165 per kWh), but their lifetime is limited up to only 300 cycles, and will thus require that the battery is replaced more frequently, increasing the long-term cost.

3.1.2. Nickel-based

Several nickel-based battery chemistries are known, the oldest one being the toxic Nickel-Cadmium (Ni−Cd) chemistry, which is banned in the EU. The most promising nickel-based battery chemistry is the nickel-metal hydride (Ni−MH) type with the negative electrode consisting of a hydrogen-absorbing alloy, the positive electrode containing nickel-hydroxide ($Ni[OH]_2$), and the electrolyte being alkaline. The practical energy density of Ni−MH battery cells is approximately 60–80 Wh/kg and its nominal cell voltage equals 1.2 V [4, 6].

Ni-MH batteries support charging up to 1C and discharging up to 2C [13]. Their charge-discharge efficiency lies between 66–92 % [14]. Self-discharge is a big issue with these batteries, going up to 30 % per month [11]. Although there are "low-capacity" Ni-MH batteries that have much lower self-discharge (≤10 % per month) [15], they are still in development and lower capacity than the normal "high-capacity" Ni-MH batteries. Unlike lead-acid batteries, Ni-MH batteries need to be carefully protected against overcharging because of potential temperature rise. They can also produce hydrogen gases in case of overcharging and will need vents to release these gases, similar to lead-acid batteries. They can be used between −10 °C and 60 °C. "Low-capacity" Ni-MH batteries have a cycle life of up to 3000 cycles, whereas the normal, "high-capacity" Ni-MH batteries only last up to 500 cycles [11, 13].

3.1.3. Lithium-ion

Lithium-ion (Li-ion) batteries have become widely known in the industry nowadays. Different structures are used for the cell parts with the electrolyte commonly consisting of a carbonate [4, 9, 16]. The negative electrode is mostly made of a form of graphite (C_6). Another negative electrode chemistry of the Li-ion battery is lithium titanate ($Li_4Ti_5O_{12}$), which allows faster charging than graphite, but has a reduced cell voltage of 1.4 V resulting in a reduced energy density [4, 16]. The positive electrode of Li-ion battery cells can be made of lithium cobalt oxide (Li_xCoO_2), the cheaper and safer lithium manganese oxide ($Li_xMn_2O_4$), and the low-cost lithium iron phosphate (Li_xFePO_4), which has a reduced cell voltage of 0.5 V resulting in a lower energy density [4, 16]. The practical energy density of Li-ion battery cells ranges between 80–160 Wh/kg and its nominal cell voltage equals 3.7 V. The cell voltage can decrease to 3.0 V during discharging [6].

Li-ion batteries support charging and discharging up to at least 4C [10] without significantly impacting the charge/discharge efficiency, which lies between 80–90 % [17]. Self-discharge is less than 10 % per month. Similar to the Ni-MH battery, overcharge is an issue, and protection against it needs to be carefully designed. Li-ion batteries only operate well between 0 °C and 60 °C, although the upper limit generally is set much lower (45 °C due to the flammability of the liquid electrolyte). Charging below freezing temperature does not only reduce efficiency, but it can also cause permanent damage to the battery cell [10]. Initial costs are relatively high (€330 to €580 per kWh), but due to its long lifetime of up to 3000 cycles, it is cheaper than other battery types over a longer period of time.

3.1.4. Comparison

The advantages and disadvantages of the discussed battery types are summarized in Table 3.1.

3.2. Battery design

The combination of individual cells forms a battery pack that shall meet the requirements. For cells placed in series, the cell voltages add up such that a higher potential can be reached. Placing cells in parallel increases the maximum current draw while the voltage stays the same. In both cases, the amount of energy (in Wh) available is still the same and depends only on the number of cells and the amount of energy in each cell.

3.2.1. Requirements

Given the BMS system requirements from Chapter 2.2, firstly, the battery shall be able to deliver at least enough energy to charge (0–100 %) an average phone twice (which requires 25.9 Wh, based on an average capacity of 3500 mAh, at 3.7 V). Taking the absolute minimum wireless charging efficiency into account (50 %), 51.8 Wh is required. Secondly, the battery shall be able to deliver enough energy for the disinfection module (which requires on average 1.5 Wh [1] each charge cycle). Furthermore, the battery output shall have an output bus with at least 15 V. Given the trade-off requirements from Chapter 2.2, the battery weight and costs should be minimized while the capacity should be maximized.

Table 3.1: Property comparison between the discussed battery types.

Property	Lead-acid	Ni-MH	Li-Ion
Specific energy (Wh/kg)	35	60–80	80–160
Nominal voltage (V)	2.0	1.2	3.7
Charge-discharge efficiency (%)	50–85	66–92	80–90
Maximum charging rate (C)	0.25	1	>4
Maximum discharging rate (C)	0.1[a]	2	>4
Self-discharge per month (%)	5	30[b]	<10
Cycle life (to 80% of initial capacity)	300	500[b]	3000
Operating range (degrees Celsius)	−20 to 60	−10 to 60	0 to 60[c]
Chemical stability	Medium	High	Low
Overcharge tolerance	High	Low	Low

[a] Sustained discharge
[b] For normal ”high-capacity” batteries
[c] Generally set lower for safety

3.2.2. Topology

In Section 3.1.4, the promising battery chemistries were compared. The specific energy of Li-ion batteries is found to be the highest compared to the lead-acid and Ni−MH chemistries. Regarding charging and discharging, the Li-ion battery can also reach rates larger than 4C, whereas the other types only reach 0.25C and 1C. The efficiency of Li-ion competes in the higher (dis)charging efficiency range of Ni−MH. In terms of self-discharge per month and temperature operating range, the lead-acid battery is most favorable. Li-ion batteries have the smallest temperature operating range and score badly on chemical stability and overcharge tolerance.

The system functional requirement [**F.3.1**] specifies one output with at least 15 V. Since the cell voltages fluctuate depending on SoC, designing the battery voltage for at least 15 V reduces the need for a step-up converter. Furthermore, having a higher battery potential reduces the current needed for constant power, which reduces the losses in the wires and the required thickness of the wires.

The trade-off requirements [**T.1**] and [**T.4**] indicate that the battery weight should be minimized and capacity maximized. This makes the Li-ion chemistry the best option based on specific energy. With a nominal cell voltage of 3.7 V, and 3.0 V discharged, it also requires only 5 series cells in order to have at least the required 15 V in all conditions. For lead-acid and Ni-MH, respectively 8 and 13 cells are required to obtain the required potential considering nominal cell voltages. Furthermore, the achievable charge and discharge rates are also much lower for lead-acid and Ni-MH battery cells. As mentioned in Section 3.1.3, Li-ion configurations with different cell voltages exist. The electrolytes can be made of different materials. For the lithium-iron-phosphate, the nominal cell voltage is reduced to 3.2 V. Consequently, the cell voltage when discharged is reduced such that more cells are required to obtain at least 15 V. This makes the nominal cell voltage around 3.7 V required.

Following from system functional requirements [**F.3**] and [**F.4**], at least 51.8 Wh is required to charge an average phone battery twice, plus an additional 1.5 Wh for disinfecting, totalling 53.3 Wh. However, due to general losses (converter efficiency, heat dissipation losses in wires, etc.), more energy than this baseline will be needed. The wireless efficiency has been estimated at the absolute minimum of 50 % [2]. Since each Li-ion battery cell has 12.6 Wh energy (based on 3500 mAh at 3.6 V), the absolute minimum amount of cells needed is 5 cells. This makes the topology 5S1P (5 series, 1 parallel).

3.2.3. Selection

The battery chemistry was selected as Li-ion with a 5S1P configuration in Section 3.2.2. Commercially available Li-ion battery cells are presented in Table 3.2. The selection is made from the websites of Farnell, Mouser, and RS-online.

Table 3.2: Selection of commercially available battery cells.

Type	Capacity [mAh]	Voltage [V]	Charge [mA]	Discharge [mA]	Self discharge [%]	Price [€/pc]
1307-0000	2600	3.6	1300	5000	10	22.25
1307-0001	3500	3.6	1700	5000	10	29.09
1307-0002	2600	3.6	2600	5000	10	24.92
1307-0003	3400	3.6	1625	4875	10	33.24
2347-3003	2600	3.7	2500	2500	20	24.99
2347-3008	2600	3.6	2500	2500	20	31.16
2347-3008-20	3500	3.6	2500	2500	20	38.24

For 5S 3.6 V battery cells, at least 3044 mAh per cell is required. For 5S 3.7 V battery cells, at least 2962 mAh per cell is required. Cell types: 1307-0001, 1307-0003 and, 2347-3008-20 meet the capacity requirements. Based on the trade-off requirements [**T.2**] and [**T.4**], the 2347-3008-20 battery type is the most promising. It has the highest capacity of 3500 mAh, with a moderate discharging current of up to 2500 mA. For discharging this is enough since the maximum available discharging power (45.4 W) is in that case far above the required 34 W. It has the highest possible charging current of the three possible battery types. Even though its unit cost (38.24 €/pc) is relatively high, it does score the best on performance aspects.

4

Battery Charging

In the previous chapter, the battery cell and topology were selected. Now, the design of the subsequent charging system is discussed. Firstly, the USB-C input is outlined together with its implementation. Secondly, the charging methods are discussed. Lastly, the charging converter is designed and verified by simulation.

4.1. USB-C connector

As specified by system functional requirement [**F.1**], the battery shall be charged via a USB-C input using an official USB protocol. The USB Type-C is a USB connector consisting of 24 pins, including 4 power (VBUS) pins, 4 ground (GND) pins, 8 pins for super-speed differential data (TX, RX), 4 pins for high-speed differential data (D+, D-), 2 pins for channel configuration data (CC) and 2 pins for sideband use (SBU) data. The USB-C connector is rotationally symmetrical, which means that it can be plugged into in any orientation. When a connection between two devices with USB-C connectors is made, the cable orientation will be synchronized by monitoring the CC1 and CC2 pins. The layout of a USB-C connector is shown in Figure 4.1.

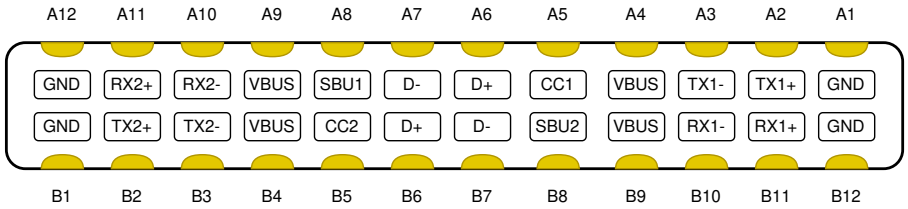

Figure 4.1: USB-C Header pin diagram.

4.1.1. Protocol

An official USB protocol shall be supported as specified by system functional requirement [**F.1**]. The USB-C standard classifies different port types [18]. For data flow, a device can be a downstream-facing port (DFP), upstream-facing port (UFP), or dual-role data (DRD) port. A DFP sends data and acts as host, a UFP receives data and acts as a device. A DRD can act as either a DFP or a UFP. For power flow, these ports can be configured as source, sink, and dual-role power (DRP) device. A source provides power on the VBUS pins. A sink draws power from the VBUS pins and a DRP device can act either as a source or sink. The configuration is communicated between both ends of the connection over the CC1 and CC2 pins.

Different USB protocol versions with power-flow capabilities are supported by USB-C compliant connectors [19–23]. A comprehensive description of these protocols is given in Appendix B.2. The main properties of these protocols are summarized in Table 4.1.

Table 4.1: Different profiles of the USB-power delivery standard.

Version	Maximum power	Voltage	Maximum current
USB 2.0	2.5 W	5 V	500 mA
USB 3.1	2.5 W	5 V	900 mA
USB 3.2	7.5 W	5 V	1.5 A
USB BC 1.2	7.5 W	5 V	1.5 A
USB-Type C 1.2	15 W	5 V	3 A
USB-PD	100 W	5/9/15/20 V	5 A

In Section 3.2.3, the battery cell type was selected. This battery has a recommended charging current of 1.75 A [24]. For the 5S1P configuration, the standard charging voltage is 21 V. Following from trade-off requirement [**T.5**], the battery should be charged as fast as possible. This means that the USB-PD protocol is most favorable since it supports a power transfer at the desired value of $1.75\,\text{A} \cdot 21\,\text{V} = 37\,\text{W}$.

4.1.2. Specifications

As specified in the USB-PD standard [22], several power rules have to be followed when designing a USB-PD compliant device. These rules define four voltage levels: 5, 9, 15, and 20 V. When a USB-PD connection is made, the lowest power transfer is initiated first (5 V, 900 mA). If the source advertises higher power transfer capabilities, the sink may draw more power if it supports the advertised quantity. Sources shall be able to supply all levels below the maximum power output (i.e. sources able to supply 27 W shall support 5 and 9 V). The source shall advertise its power delivery capabilities. A sink may not draw more current than a source advertises over the CC lines. The power rules are illustrated in Figure 4.2.

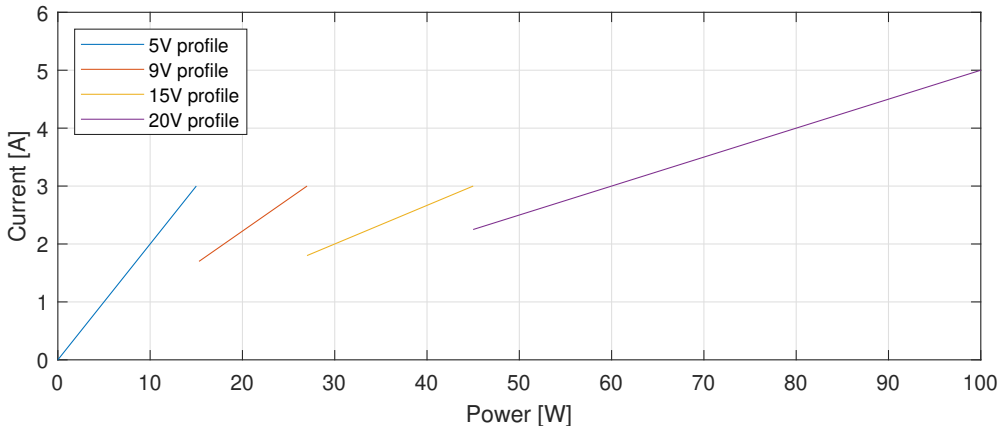

Figure 4.2: USB-PD power profiles as specified by the USB-PD standard [22].

The individual battery cells have a capacity of 3500 mAh and a voltage of 3.635 V. When discharged, the cell voltage equals 3 V and when fully charged 4.2 V. Therefore, the 5S1P topology battery voltage range is in between 15–21 V.

Since the battery voltage is not equal to the USB-PD power rule voltages and the battery charging process needs to be controlled, a converter is needed. This converter can be step-up, step-down or both step-up/step-down. For the 5 and 9 V power rule, only a step-up converter is needed. When 15 and 20 V power rule are used, a step-up/step-down converter is needed. The efficiency for a step-up converter is in general higher than for a step-up/step-down converter [25]. Therefore, the 9 V power rule is chosen.

4.1.3. Driver

As specified, the charger needs to be charged via a USB-C connector. The chosen protocol is USB-PD with the 9 V power rule. At this power rule, the maximum power draw is 27 W. The USB-PD protocol requires a driver that is able to detect the amount of power that may be drawn. For the driver, the simplest model is a UFP since the only requirement is that it needs to be charged via a USB-C connector with an official USB protocol [18]. The functional model of a UFP is shown in Figure 4.3.

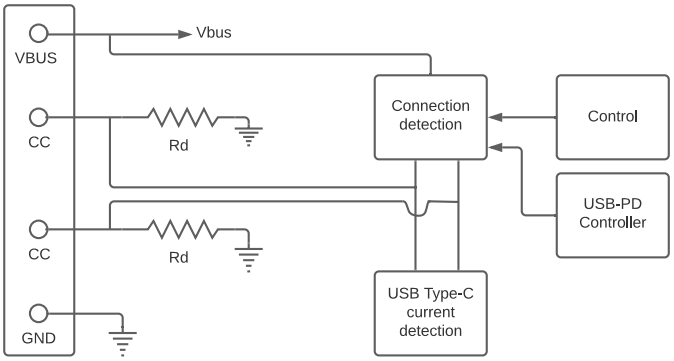

Figure 4.3: Functional diagram of a USB-C upstream facing port.

The CC pins shall be terminated to ground via pull-down resistors (Rd). The VBUS pins shall be monitored to detect a connection with a source. According to the voltage drop over the resistors, the maximum power draw advertised by the DFP can be determined. The cable orientation should be taken into consideration since both CC lines have different voltage specifications indicating the power draw advertisement. For USB-PD, a dedicated controller is needed for connection detection and negotiation with the DFP about the power draw. Several USB-PD drivers satisfying the requirements are presented in Table 4.2.

Table 4.2: Commercial USB-PD drivers, selection from [26].

Type	Maximum power [W]	Controller	Price [€/pc]
STM32L5x2	100	internal	3.76
STUSB4500	100	internal	1.48
TPS65983B	100	external	8.63
TUSB321	15	internal	1.98
TUSB422	100	external	1.23

Based on the available drivers presented in Table 4.2, it can be seen that the STM32L5X2 and STUSB4500 support at least the desired power draw and have an internal controller to minimize additional components. The STM32L5x2 also supports the controller requirements as specified by the UV-C module [1]. Combining the system controller and USB-PD controller reduces the number of components needed which makes it the preferred device.

Architecture For the implementation, specific I/O pins are used for the STM32L5x2 internal USB-PD driver [27]. These pins feature the necessary pull-up and pull-down resistors. The STM32L5x2 can be programmed by the use of its programming manual [28]. The IC can be supplied by the battery using a step-down converter.

4.2. Charging methods

There are several methods of charging a battery. The most well-known ones are Constant Voltage (CV), Constant Current (CC), Constant Current – Constant Voltage (CC-CV), and pulse charging [29, 30]. The method of charging is determined by the converter used between the USB-C port and the battery.

Constant Voltage The output voltage of the converter is kept constant with this method. This way, a fluctuating current will be present at the output and charge the battery. As the battery voltage nears the converter output voltage, the current will decrease until both voltages are equal, at which point the current will approach zero. This method has a low risk of overcharging if the output voltage level is set below the maximum battery voltage. The disadvantage is that the charging time is relatively long, since the current decreases over time as the battery becomes more fully charged [29].

Constant Current With this method, the converter keeps its output current constant. As a result, the output voltage will fluctuate. Since the voltage fluctuates, it becomes harder to reach 100 % SoC, decreasing the effective capacity of the battery. Another issue is overcharging, as it will not automatically stop charging when the battery reaches a set voltage level. However, since the current is set to be constant at a higher value than with CV, charging time will be relatively fast [29].

Constant Current – Constant Voltage This method combines the advantages of the two previously discussed charging techniques. First, a constant current is applied up to a certain SoC (which is usually around 60–80 %) [31], then a switch is made to the constant voltage scheme to prevent overcharging and permanent damage to the battery cells. Afterward, the charging is completely terminated when the current reaches a threshold value. This combination provides the benefit of having a lower risk of overcharging, while at the same time having relatively fast charging rates.

Pulse charging This method uses mono-phasic current pulses (i.e. square waves) to charge the battery. In comparison to just CC charging, pulse charging achieves a higher maximum SoC and a higher charging rate. On the other hand, it also increases heat generation, which can become problematic for Li-ion batteries. The circuit required for pulse charging is also more complex than the previously discussed techniques [30].

4.2.1. Charging method selection

Considering trade-off requirements [**T.5**] and [**T.4**], the battery should be charged as fast as possible and have the highest possible capacity. This makes pulse charging the most promising method as it achieves a higher maximum SoC and a higher charging rate than CC, CV, and CC-CV charging.

In order to meet safety requirement [**S.1**], charging must be done in a safe manner. The battery chemistry was selected in Section 3.2.2 as Li-ion. Since the additional heat generation of the pulse charging method may cause problematic failures for the chosen Li-ion cells, pulse charging is excluded. As a relatively fast and safe charging method, CC-CV charging will be used. This method combines the benefits of both CC and CV charging to obtain higher performance in charging time, whilst ensuring safety.

For the implementation of CC-CV charging, a DC-DC converter is typically used directly for constant-voltage regulation [32]. The duty cycle can be adjusted to match the desired output voltage. Current feedback is applied alongside the DC-DC converter to implement constant-current control. The duty cycle can then, similarly to constant voltage regulation, be adjusted to keep the output current at the desired value.

4.3. Converter

As mentioned in Section 4.2.1, the typical implementation of a CC-CV charger is a DC-DC converter with duty cycle regulation and current feedback. There are two types of DC-DC converters: isolated and non-isolated. Since isolated converters will require more components and a larger area, this type will not be considered by trade-off requirement [**T.2**]. The requirements, derived from the battery and USB specifications, which the converter shall meet are presented in Table 4.3.

For non-isolated converters, there are many different topologies available for use: boost, buck-boost, SEPIC, Zeta (inverse SEPIC), and Ćuk [33]. The boost converter is the most area-efficient in its task (stepping up, and non-inverting) since the other topologies are basically a combination of the buck and boost converters. This also means the SEPIC, Zeta, and Ćuk topologies do allow for both stepping up and stepping down without changing their topology. Since the required battery voltage is always higher than the input voltage, a boost converter is sufficient without adding unnecessary complexity and components.

Table 4.3: The overall requirements for the converter.

Parameter	Specification
Input voltage	9 V
Output voltage	15–21 V
Output current	1 A [a]
Control mechanism	CC-CV
Output polarity	Non-inverting
Isolation	Not required

[a] Based on the available input power, the recommended 1.75 A is not feasible. This will be explained more in-depth in Subsection 4.4.1.

4.3.1. Boost topology

The general functionality of a boost converter is that it converts a lower DC voltage to a higher DC voltage. The configuration and operation can have different forms.

Configuration There are two possible configurations for the boost converter: asynchronous and synchronous. Figure 4.4 shows these two configurations of the boost converter. The difference is in the use of either a diode (asynchronous) or an additional switching transistor (synchronous) in the conduction path to the load. The main advantage of using a synchronous configuration is that it generally has higher efficiency, due to the lower conduction losses of the transistor (as the drain-source voltage is lower than the diode forward voltage in case the MOSFET is fully conducting). However, an additional transistor also adds complexity to the circuit. The output capacitor will be shorted when both transistors are conducting at the same time. Furthermore, using Schottky diodes can decrease the efficiency gap between the two variations (although there still will be noticeable differences). Finally, the chosen controller must also support a synchronous topology, which reduces the number of options. Due to these reasons, an asynchronous design is chosen.

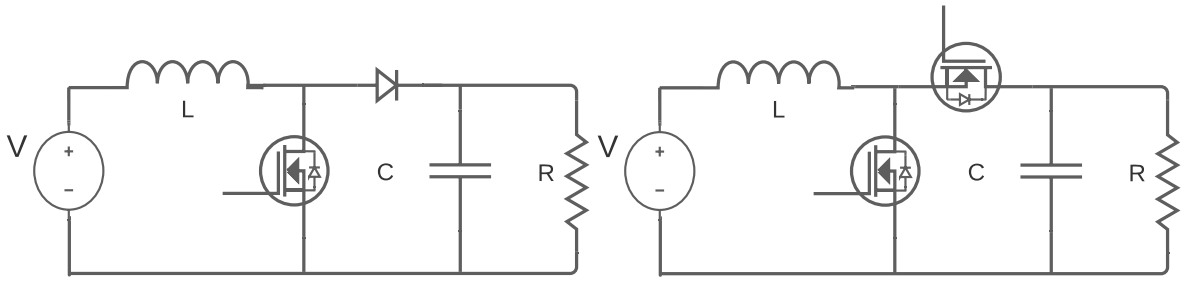

(a) Asynchronous boost converter layout. (b) Synchronous boost converter layout.

Figure 4.4: Synchronous vs asynchronous boost converter topologies.

Conduction mode In continuous conduction mode (CCM), the current through the inductor will never drop below 0 A and thus will continuously conduct. In discontinuous conduction mode (DCM), this current will clip at 0 A for a non-zero time period, and the inductor will be completely discharged during this period. Since in DCM the input to output relation becomes non-linear, staying in CCM is preferable.

4.3.2. Working principle

The output voltage of the converter can be controlled by the on-time and off-time of the MOSFET switch. When the MOSFET is in the on-state (closed), the current flows as in Figure 4.5a. The MOSFET off-state (opened) is depicted in Figure 4.5b.

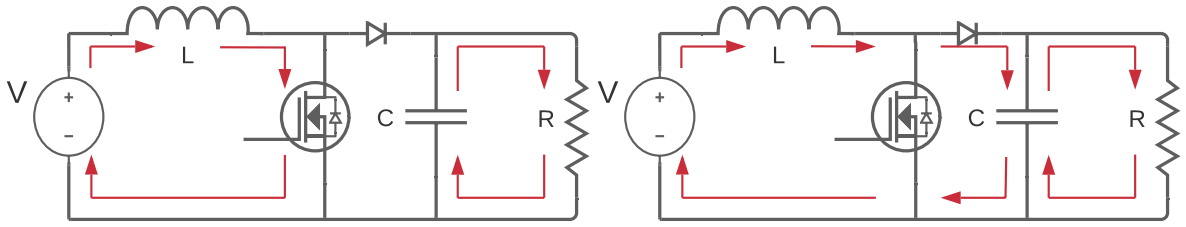

(a) Boost converter in on-state (MOSFET is closed).

(b) Boost converter in off-state (MOSFET is opened).

Figure 4.5: Boost Converter Topology.

In the on-state, the current flows from the source through the inductor and the switch to ground. The diode current (I_d) equals zero and the voltage over the inductor equals the source voltage, with the inductor current increasing as given in equation 4.1.

$$V_L = L \cdot \frac{\partial i}{\partial t} = V \tag{4.1}$$

When the switch is in the off-state, the diode current equals the inductor current, and the voltage over the inductor will be the difference of the source and output voltage: essentially the inductor will act as a current source, and thus steps up ("boosts") the output voltage over the load. The output voltage then depends on the input voltage, the duty cycle of the switch, and the efficiency (η) of the components:

$$V_{out} = \frac{V_s}{1 - D} \cdot \eta_{total} \tag{4.2}$$

Since the output voltage is stepped up, the output current must be stepped down with the same ratio, as otherwise there will be a power imbalance. The output current can then be found as:

$$I_{out} = \frac{I_L \cdot V_s}{V_{out}} \tag{4.3}$$

4.3.3. Theoretical design

In this section, the theoretical background and equations of a boost converter will be discussed.

Ripple Due to the way the boost converter continuously charges and discharges the inductor, the current and output voltage will not be completely constant. It will decrease and increase every cycle, and thus also depends on the switching frequency: the lower the frequency, the higher the deviation. This deviation from the average signal is called the ripple. Even though the output ripple does not affect the performance and lifetime of a battery [34], care must be taken to ensure that the peak output (constant voltage/current + ripple) is still below the maximum rating of the battery.

The current ripple will be dependent on the inductor value, and the output voltage ripple will be dependent on the capacitor value. More specifically, since the time-averaged voltage across the inductor must be zero for one cycle (when in steady state), for the inductor current ripple:

$$\Delta I_L = \frac{V_s \cdot D}{f_s \cdot L} \tag{4.4}$$

Similarly, since the time-averaged current through the capacitor must be zero for one cycle (again, when in steady state), for the output voltage ripple:

$$\Delta V_{out} = \frac{I_{out} \cdot D}{f_s \cdot C} \tag{4.5}$$

However, the equivalent series resistance (ESR) of the capacitor also adds additional output voltage ripple [35]:

$$\Delta V_{out,ESR} = ESR \cdot \left(I_{out,max} + \frac{\Delta I_L}{2} \right) \tag{4.6}$$

Switching frequency Since the supply voltage is constant (USB output), and the duty cycle D is already designed for in other parameters (such as output voltage), it can be seen that the switching frequency f_s and inductance L need to be chosen. The switching frequency does not have a hard requirement, but some trade-offs should be considered. A lower frequency will result in a higher ripple and the need for larger passive components that will have more passive losses. A higher frequency will require faster switching MOSFETs and increase switching losses.

Inductor As explained in Section 4.3.1, it is preferable that the inductor remains in CCM. To this end, the inductor must be above a minimum value to avoid that the current drops below zero due to the ripple. This means that:

$$\Delta I_L < 2I_L \tag{4.7}$$

Then the minimum value for the inductor is:

$$L_{min} = \frac{D \cdot V_s}{f_s \cdot 2I_{L,min}} \tag{4.8}$$

Diode As mentioned before, an asynchronous topology is chosen, and hence the diode needs to be chosen carefully. The diode needs to capable of dissipating the power in conduction mode:

$$P_d = V_F \cdot I_F \tag{4.9}$$

Where the forward current I_F represents the output current I_{out}. The highest instantaneous P_d will be at peak $I_{L,max}$. The diode also needs to be capable of handling this peak current, however, most Schottky diodes will have a high enough peak current rating [35]. Schottky diodes should be used anyway, as they not only have a lower forward voltage than normal p-n junction diodes but also do not have a reverse recovery time [36], both of which will reduce losses significantly. On the other hand, Schottky diodes do have a higher junction capacitance C_j, which can increase switching losses of the MOSFET:

$$P_{j,loss} = \frac{C_j \cdot V_{reverse}^2}{2f_s} \tag{4.10}$$

MOSFET The MOSFET switch has to be able to handle the peak current:

$$I_{sw,max} = \frac{\Delta I_L}{2} + I_{max,L} \tag{4.11}$$

Furthermore, it must be able to block the voltage across it in its off-state:

$$V_{sw,min} = \frac{\Delta V_{out}}{2} + V_{max,out} + V_f \tag{4.12}$$

The MOSFET should be chosen such that its maximum current and voltage rating are above these minimum values, with a safety margin of 30 %. It should also be able to switch fast enough.

4.4. Design

In this section, the design of both the boost converter and the converter control will be discussed.

4.4.1. Overall charging requirements

First, the overall requirements of the total charger (e.g. charging current, switching frequency) must be discussed, as these are necessary for both the design of the CC-CV control (Section 4.4.2) and the boost converter (Section 4.4.4).

The recommended values for charging the batteries (found in the datasheet of the chosen battery [24]) for the two phases (CC and CV) can be seen in Table 4.4.

The recommended end current specified in the datasheet is 35 mA. However, for this charger, an end current of 175 mA will be used. The reason for this is that the lower the end current is, the shorter the lifetime of the battery will be. Consequently, it will have a lower SoC, but the difference in SoC and

Table 4.4: Battery charging specifications of the 2347-3008-20.

Parameter	Specification
Recommended charging current	1.75 A
Maximum charging current	2.5 A
Standard charging voltage	21 V
End current	175 mA[a]

[a] Recommended is 35 mA, however this will not be used. See text for the explanation.

the difference in lifetime justify the higher end current [37]. With the chosen end current, an SoC of more than 99 % can still be reached.

Based on the power available through the USB connection, it is not possible to reach the recommended charging current in CC-mode, as 1.75 A at 21 V is well above the available 27 W. Therefore, the charging current is set close to the highest possible value instead (taking into account efficiency/losses), which is 1 A.

Switching frequency Another requirement that has to be chosen beforehand is the switching frequency f_s. As explained before in Section 4.3, this does not have a strict requirement but trade-offs that need to be kept in mind. To prevent unwanted noise for the wireless-charging subgroup [2], the switching frequency needs to be outside their operating range (which is 80–200 kHz [2]). Since the switching MOSFET is integrated into the charging IC, and there is little information about its switching characteristics, the switching frequency is taken as low as possible. However, the IC cannot output a constant frequency. The datasheet shows that this can deviate by 10 % below and above the set frequency. In order to ensure that it remains above 200 kHz, a frequency of 250 kHz is chosen.

4.4.2. Boost control

There are several integrated circuits available on the market that facilitate CC-CV charging by means of converter regulation. Potential models with their properties are listed in Table 4.5.

Table 4.5: Various DC-DC converter regulators ICs available on the market.

Model	Topology	Frequency [kHz]	Current-sensing	FET	Configuration
LM5022	Boost, SEPIC	200 - 2200	Inductor	external	asynchronous
LT3579	Boost, SEPIC	200 - 2000	Inductor	external	asynchronous
LT3956	Buck, boost, buck-boost	100 - 1000	Inductor or load	internal	asynchronous
LTC3786	Boost	50 - 900	Inductor	external	synchronous

All models mentioned in Table 4.5 could be used as a converter regulator, and support the overall requirements as given in Table 4.3. The LT3956 allows load current-sensing as opposed to only inductor current-sensing, making current regulation much more precise. A disadvantage of the LT3956 is that it has an internal switch, and thus the switch cannot be specifically designed and chosen for the exact functionality needed (it is now designed to work in a broader range of values for voltage, current, etc. than needed). However, a reasonable assumption is that the losses have been taken into consideration in the given frequency range. Furthermore, having an internal switch can help reduce costs and area size. The advantages of having load current-sensing available outweigh the potential extra MOSFET losses (see Appendix B.3 for the loss calculation), and thus the LT3956 is selected as the converter controller.

4.4.3. LT3956 configuration

The LT3956 needs external components connected to several of its ports. The values of these components will be discussed in the following paragraphs.

Switching frequency As per Section 4.4.1, the switching frequency had been set to 250 kHz. The LT3956 allows setting the frequency by use of an external resistor R_T. The datasheet provides a figure with the switching frequency plotted against the resistance value. The value for R_T is estimated using this figure as:

$$R_T = 43\,\text{k}\Omega$$

Enable/Undervoltage detection The EN/UVLO pin allows the user to set a rising and falling voltage level at which the IC enables or disables itself. This is done by using a 2.1 µA pull-down current when below the falling voltage level and thus increasing the rising level.

$$V_{falling} = 1.22\,\text{V} \cdot \frac{R1 + R2}{R2} \qquad V_{rising} = 2.1\,\mu\text{A} \cdot R1 + V_{falling} \tag{4.13}$$

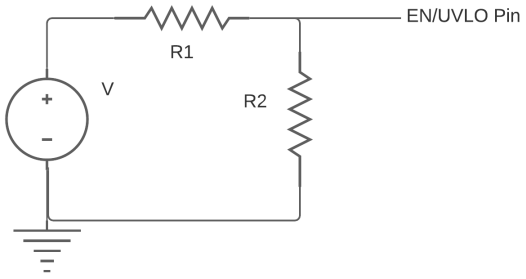

Figure 4.6: Resistive divider to the EN/UVLO pin.

With R1 and R2 being the resistors as shown in Figure 4.6. Since hysteresis is not necessary, it will not be specifically taken into account during design. However, it should be noted that it is present, and the rising voltage level should be below the input voltage or else it will never turn back on. By using a resistive divider, undervoltage of the input source can be detected. The undervoltage limit will be set at 8.5 V. Since the falling threshold is 1.22 V, the divider will have the resistors:

$$R1 = 60\,\text{k}\Omega \quad \text{and} \quad R2 = 10\,\text{k}\Omega$$

which gives the final voltage levels of:

$$V_{rising} = 8.67\,\text{V} \quad \text{and} \quad V_{falling} = 8.54\,\text{V}$$

Soft-start The LT3956 allows for soft-start, which prevents high inrush currents when starting the circuit and consequently limits the rate at which the output voltage rises. This protects the components from excessive peak currents. The soft-start interval can be set by using an external capacitor C_{ss}. The datasheet mentions a 10 µA pull-up current towards an internal 2.5 V rail. This means the capacitor will be charged towards the internal rail. The soft-start finishes when 2 V is reached, as this voltage is compared to a separate internal value. The time spent reaching this value is:

$$t_{ss} = \frac{2 \cdot C_{ss}}{10\,\mu\text{A}} \tag{4.14}$$

The datasheet recommends a C_{ss} of 10 nF, which would result in a t_{ss} of 2 ms.

Loop compensation With additional loop compensation, the inductor and output capacitor can be chosen purely based on cost, size, and performance. It is possible to use an external capacitor and resistor at the output of the internal error amplifier to compensate the control loop and ensure loop stability (Type 2 compensation without an extra parallel capacitor). The datasheet does not give an exact formula for the values of these components, and only recommends a value of 4.7 nF. However,

testing in LTspice showed that this was insufficient and resulted in oscillations in the output voltage and current. Using the following parameters, the oscillation was no longer present in the simulation:

$$C_{comp} = 50\,\text{nF}$$

$$R_{comp} = 1.5\,\text{k}\Omega$$

Operation mode The LT3956 has a pin that shows the current operation mode of the charger: namely either CC or CV. It requires an external pull-up resistor. Since the resistor will be connected to a pin that regulates its output to 7.15 V and a maximum current of 1 mA is allowed, a resistor with the following minimum value is needed:

$$R_{min} = 7.15\,\text{k}\Omega \tag{4.15}$$

Output voltage regulation The output voltage regulation can be set to the constant voltage level required, which is 21 V. The controller will regulate the duty cycle based on the voltage present at the FB pin and will regulate this towards 1.25 V. So then a simple resistive divider (see Figure 4.7) can be used to regulate the output voltage:

$$V_{out} = 1.25\,\text{V} \cdot \frac{R1 + R2}{R2} \tag{4.16}$$

which gives the following resistor values:

$$R1 = 158\,\text{k}\Omega \quad \text{and} \quad R2 = 10\,\text{k}\Omega$$

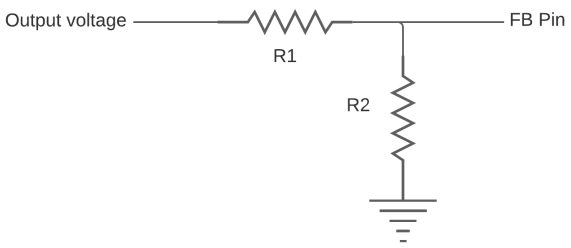

Figure 4.7: Resistive divider from output to the FB pin.

Output current regulation The output current regulator in the LT3956 will regulate the output current. The current value to which it will regulate depends on the current-sensing resistance as the LT3956 limits the voltage over this resistor to 250 mV, and hence the average current through this resistor according to:

$$I_{max} = \frac{250\,\text{mV}}{R_{sense}} \tag{4.17}$$

which, for a current of 1 A gives a sense resistor of:

$$R_{sense} = 250\,\text{m}\Omega$$

4.4.4. Component requirements

In this section, the design of the components in the boost converter will be discussed.

Inductor In order to keep the inductor in CCM, the inductor current ripple must conform to equation 4.7. In this case, I_L in this case will be the lowest required output current. This output current will be the 175 mA mentioned above (i.e. the stopping current in CV-mode). Using equation 4.3, and using the ideal efficiency η_{total} of 100 % for the lowest inductor current, this results in an average I_L of 408.3 mA.

Then, the maximum ripple allowed will be around 816.6 mA. First, the maximum duty cycle must be found, so that the minimum inductor value can be calculated using equation 4.8. The maximum duty cycle will result in the highest output voltage, as per equation 4.2. Since the highest output voltage required is 21 V, and the worst-case efficiency η_{total} is 80 % [35], the maximum duty cycle is 0.66 according to equation 4.2. Then finally, the minimum inductance value needed is 29.1 µH.

Output capacitor Similarly, the output voltage ripple must not cause severe overcharging of the battery. The absolute maximum rating of the battery used is 4.325 V per cell [24]. Therefore, an additional 125 mV is allowed over the constant voltage value per cell, i.e. a ripple of 250 mV is allowed per cell. With five cells, this gives a maximum voltage ripple of 1.25 V. The voltage is determined by the capacitance and its ESR (see equation 4.5 and equation 4.6). It is best to therefore use a capacitor with a low ESR. Since the contribution of the ESR to the voltage ripple for sufficiently low ESR capacitors (i.e. less than 100 mΩ at 250 kHz) is negligible (less than 0.1 V), the minimum capacitance can be calculated, using $D = 0.66$, $I_{max,out} = 1.07A$, which gives a value of 2.2 µF. Note that this is the absolute minimum, and it is advisable to be well above this value after taking into account tolerance and variability (i.e. 5x this value).

MOSFET switch The MOSFET switch has to be chosen such that it can handle the switching frequency, the peak current during conduction, and the reverse recovery current during switching. The peak current can be calculated using equation 4.11. This gives a maximum current of 3.07 A, however, due to switching mechanisms and overshoot the rating should be well above (30 %) this value, giving a minimum current rating of 4 A.

The maximum voltage the MOSFET needs to be able to handle when it is off is found using equation 4.12. This is the sum of the maximum output voltage, maximum ripple, and the forward voltage V_F, which is 22.45 V. Adding the safety margin of 30 %, the final minimum voltage rating of the MOSFET is 29.2 V.

Diode Finally, the diode must be able to dissipate the power without overheating (see Section 4.6 for more details). Since every Schottky diode will have a slightly different forward voltage (150–800 mV), this will have to be judged case to case. Although in the best-case scenario of 150 mV, the diode will need to dissipate 160.5 mW (see equation 4.9). Furthermore, the diode needs to be able to handle the maximum reverse voltage across it, and the maximum forward current through it. The maximum reverse voltage over the diode is, similar to the MOSFET voltage rating, the maximum output voltage of 21 V. The maximum average current through the diode will be $I_{out,max}$, which results in a minimum average current rating of 1 A. Taking a 30 % safety margin into account, a minimum voltage rating of 27.3 V and a minimum average current rating of 1.3 A is required.

The parameters and their values explained in the text above, are summarized in Table 4.6.

4.4.5. Component selection

With these component requirements, components can be selected. This will be done in the following paragraphs.

Inductor Aside from the parameters described above, the inductor ESR is also very important. While this does not have a strict requirement, it should be as low as possible to reduce losses. Table 4.7 shows a selection of the commercially available inductors.

The inductor chosen is the Kemet MPXV1D1250L680 [38]. While other inductors can have even lower ESR, they are much more expensive and generally take up more space, and are thus not considered for this design. However, if the highest possible efficiency is desired with disregard to the cost and size, the Kemet MPXV1D2213L680 [39] can be considered, as it only has an ESR of 30.8 mΩ.

Table 4.6: The parameters needed for the design of the boost converter.

Parameter	Value
Maximum inductor current ripple	816.6 mA
Maximum output voltage ripple	1.25 V
Minimum inductance	29.1 µH
Minimum capacitance	2.2 µF[a]
Minimum voltage rating switch	29.2 V
Minimum current rating switch	4 A
Minimum power rating diode	160.5 mW[b]
Minimum voltage rating diode	27.3 V
Minimum current rating diode	1.3 A

[a] Given an ESR of less than 100 mΩ
[b] Given a forward voltage of 150 mV

Table 4.7: Selection of inductors available on the market.

Inductor	Inductance [µH]	ESR [mΩ]	Current Rating [A]	Cost [€]
Bourns SRP1040VA-680M	68	210	3.5	1.37
Kemet MPXV1D1250L680	68	163	3.6	2.97
Kemet MPXV1D2213L680	68	30.8	12.5	10.27
Vishay / Dale IHLP4040DZER900K5A	90	252	3.5	1.47

Capacitor Table 4.8 shows a selection of capacitors available on the market that are considered.

Table 4.8: Selection of capacitors available on the market.

Capacitor	Capacitance [µF]	Dielectric	ESR [mΩ]	Voltage Rating [V]	Cost [€]
AVX 12065D106KAT2A	10	X5R	6	50	0.48
Murata GRT31CR61H106KE01L	10	X5R	20	50	0.58
TDK C3216X5R1H106K160AB	10	X5R	15	50	0.72
TDK CNA5L1X7R1E106K160AE	10	X7R	15	25	1.13

The capacitor chosen is the AVX 12065D106KAT2A [40]. The reason for this is its lower cost for the same performance as the other mentioned capacitors. Taking into account the DC bias ($-70\,\%$), this capacitor will give an $\Delta V_{out} = 941.6\,\text{mV}$, which is below the maximum of 1.25 V.

MOSFET Since the MOSFET is integrated into the control IC, this component does not have to be selected individually. This internal MOSFET should, however, adhere to the requirements set above. The internal MOSFET of the chosen IC has a voltage rating of 84 V, and a maximum current rating of 4.6 A [41]. It supports switching up to 1 MHz and has an on-resistance of 90 mΩ. Thus it satisfies the minimum values for the parameters.

Diode Table 4.9 shows a selection of commercially available Skottky diodes that are considered.

The Schottky diode chosen is the Nexperia PMEG3020BER [42]. Aside from the parameters seen in Table 4.9, it can handle peak currents up to 50 A, has a worst-case reverse current of 50 µA, and can dissipate up to 1.8 W. This is sufficient since the peak power is $460\,\text{mV} \cdot 1.07\,\text{A} = 492.2\,\text{mW}$.

Table 4.9: Selection of Schottky diodes available on the market.

Diode	V_F [mV]	Capacitance [pF]	Voltage Rating [V]	Current Rating [A]	Cost [€]
Nexperia PMEG3020BER	460	<60	30	2	0.31
Nexperia PMEG3050BEP	450	<275	30	5	0.39
ROHM RB088LAM-30TR	690	<150	30	5	0.38

4.5. Simulation

This section describes the simulations performed for the converter setup. First, the ideal behavior is simulated in Simulink. Then, the designed converter with its controller is simulated in LTspice. Lastly, the simulations are compared to see if the expected behavior is met.

4.5.1. Simulink

The converter has been modeled as an average model at the system level. Appendix E.3 shows the simulation diagram. Equation 4.2 is used for the converter model where the efficiency has been taken unity. This means that the output voltage of the model scales with the duty cycle. The current that flows through the resistor is mapped to the input current by the same scaling factor.

For the battery model, the Simulink generic battery model has been used. The error between model and reality is below 5 % for an SoC between 10–100 % [43]. Therefore, the initial SoC has been set at 10 % in the simulation. The battery has been connected to the charger with two ideal switches in order to disconnect it when the end current of 175 mA has been reached.

The duty cycle control mechanism has been modeled with two PI controllers. The first controller saturates to the constant current limit while the battery voltage is below the desired constant voltage threshold. As a result, the second controller regulates the duty cycle for constant current mode. When the desired battery voltage is reached, the first controller is not longer saturated and now regulates the duty cycle for constant voltage mode. The simulation results for the battery current, voltage, and SoC are shown in Figure 4.8.

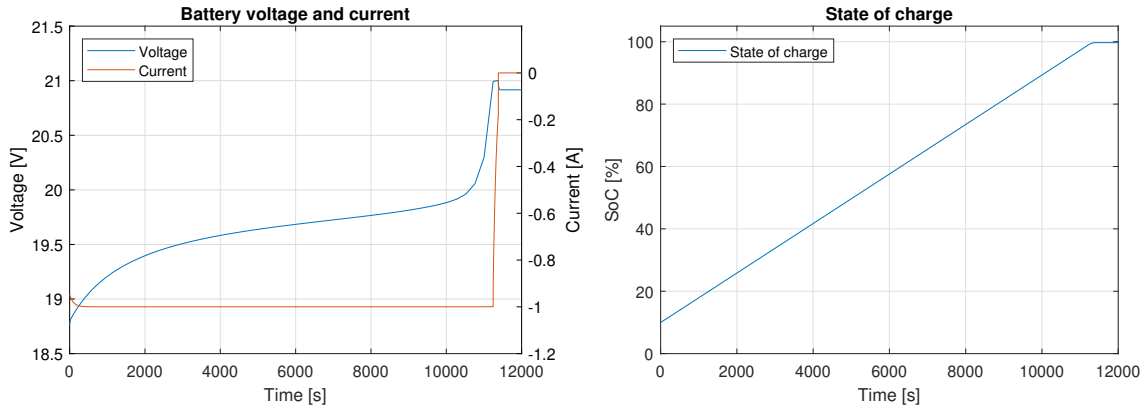

(a) Battery voltage and current during CC-CV charging.

(b) Battery SOC during CC-CV charging.

Figure 4.8: Simulink simulation results of CC-CV charging.

As seen in the simulation results, the battery SoC increases during charging. The current is monitored as the outgoing battery current, which means that during charging it is negative. The CC mode with a current equal to 1 A can be seen clearly. The battery voltage starts increasing non-linearly first, followed by a linear pattern. This corresponds to the expected behavior of the battery model [43]. After approximately two and a half hours, the battery voltage increases exponentially.

In Figure 4.9 it can be seen that when the CV voltage of 21 V has been reached, the voltage is kept constant. The current now decreases till it is less than the specified end-current of 175 mA. Here, the charger is disconnected from the battery. It can be seen that the current steps to zero, resulting in a small decrease in battery voltage. This is because the battery is charged at a higher potential than its

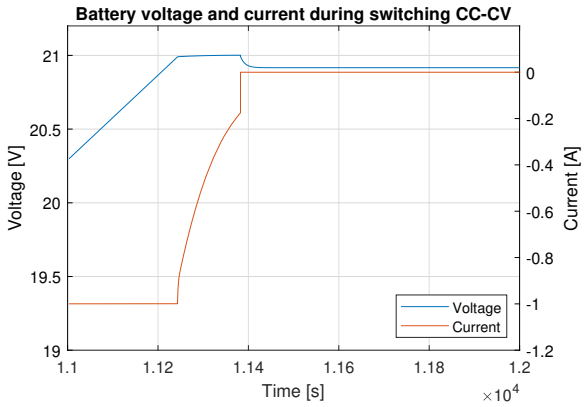

Figure 4.9: Battery voltage and current enlarged during switching from CC to CV mode.

nominal voltage. When the end current is reached, the SoC almost equals 100 %. The total charging time in this ideal case can be estimated to be around 3 hours.

4.5.2. LTspice

The setup for the LTspice simulation can be found in Appendix E.4. The USB-C input connection is modeled by a 9 V voltage source. Since the maximum input current possible is 3 A, the drawn current should be checked to satisfy this requirement in each simulation.

The battery is modeled as a voltage source with a series resistance. In order to simulate the increasing resistance of the battery as it gets charged, the resistance value of this series resistance is exponentially increased in time via a behavioral source, see Appendix E.4 for the implementation.

With this setup, the efficiency, output current, and output voltage can be plotted. These can be seen in Figure 4.10. As can be seen, the battery starts charging up to 21 V with a constant current of 1 A after the initial start-up is complete. When it nears this voltage, the converter switches to CV mode and keeps the output voltage constant. The current then decreases as a result.

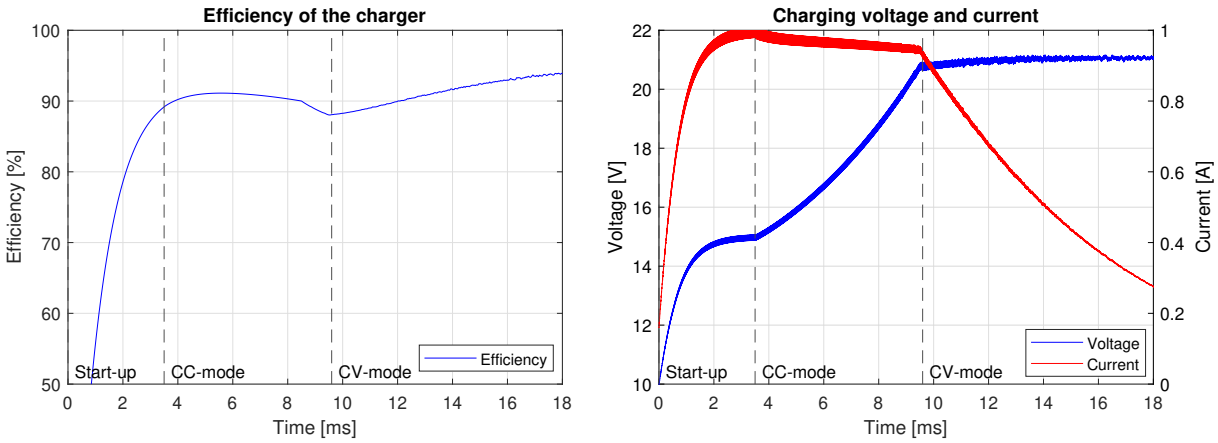

(a) Converter efficiency.

(b) Output current.

Figure 4.10: LTspice results of the converter simulation. Note that there is no end-current, as this has not been implemented in LTspice, and that the time scale is not realistic.

The exact frequency, output voltage ripple, inductor current ripple, and efficiency in each mode (both CC- and CV-mode), are shown in Table 4.10.

Table 4.10: Numerical results from the LTspice simulation.

Parameter	CC-mode	CV-mode
Frequency	259.7 kHz	259.7 kHz
Efficiency	92.8 %	94 %
Inductor current ripple	226 mA	270 mA
Output voltage ripple	215 mV[a]	186 mV[a]

[a] The DC Bias of the output capacitor is not modeled. In reality, the ripple will be much higher due to the reduced effective capacitance.

4.6. Thermal verification

For the components to function properly, the maximum specified (junction) temperature should be higher than the highest (junction) temperature during operation. The components for which this verification will be done are the LT3956 Controller IC, the inductor, the Schottky diode, and the output capacitor, as they are directly in the power path from input to output and will thus generate the most heat.

The LT3956 datasheet shows the formula for the internal junction temperature of this IC as:

$$\Delta T_j = R_{\theta,ja} \cdot (V_{in} \cdot (I_Q + f_{sw} \cdot 7\,\text{nC}) + I_{sw}^2 \cdot 0.14\,\Omega \cdot D) \tag{4.18}$$

The theoretical junction temperature increase for the three passive components can be calculated by:

$$\Delta T_j = P_d \cdot R_{\theta,ja} \tag{4.19}$$

Here, P_d is the power dissipated (in W) by the component and $R_{\theta,ja}$ is the thermal resistance (in K/W). Table 4.11 shows the maximum junction temperature, the junction to ambient thermal resistance, the power dissipation, and the resulting temperature increase.

Table 4.11: Maximum and expected junction temperature rise

Component	$T_{j,max}$ [°C]	$R_{\theta,ja}$ [K/W]	P_d [W]	ΔT_j [°C]
LT3956 IC	125	43	0.788	33.87
Inductor	155	18.9[a]	1.467	27.73
Diode	150	220	0.46	101.2
Output capacitor	85	<30[b]	0.01	0.3

[a] Based on 40 °C rise at 3.6 A (from datasheet).
[b] Exact value cannot be found. Based on other similar capacitors. Exact value not important regardless due to low power dissipation.

5

Battery Management

In this chapter, the SoC estimation, cell balancing, and protection of the selected Li-ion battery cells are discussed. First, different SoC estimation algorithms are discussed. Then, the necessity for cell balancing is discussed and different balancing strategies are presented. After that, the battery protection features are discussed together with their implementation. Finally, the design of the SoC estimation, cell balancing, and battery protection is outlined, supported using a flowchart, and verified by simulation.

5.1. State of charge estimation

The State of Charge (SoC) of a battery is a percentage indicating how much charge is present in a battery compared to that of a fully charged battery [44]. It is needed for cell balancing and in order to meet functional requirement [**F.6**], as it is specified that the battery SoC needs to be displayed by LEDs on the outside of the Wireless Powerlizer. There are multiple methods for SoC estimations. The voltage readout method and coulomb counting method are the most promising.

Voltage readout A method to estimate the battery SoC is by using the open-circuit voltage (OCV) of the battery. The OCV represents the magnitude of the battery voltage and is needed to determine the SoC from the OCV-SoC curve. These curves are necessary but hard to obtain for different current conditions [45]. For determining the OCV from the OCV-SoC curve, the battery should be disconnected. Hence, this method is not suitable during continuous operation [46].

Coulomb counting The coulomb counting method is most used nowadays. In order to estimate the remaining SoC, the current entering and leaving the battery is integrated over time [44, 47]. By taking the charging or discharging efficiency $\eta(t)$ into account, and dividing by the nominal battery capacity C_{nom} [Ah], the remaining battery capacity is known. This is mathematically shown in Equation 5.1.

$$\mathrm{SoC}\,(t) = \mathrm{SoC}\,(t_0) - \int_{t_0}^{t} \frac{\eta\,(\tau)\,I\,(\tau)}{C_{nom}} d\tau \tag{5.1}$$

However, this method is sensitive to errors [47, 48]. First, the current draw is influenced by the battery temperature and current direction. Secondly, the accurate initial SoC value is hard to obtain and current sensors need to be very accurate. Lastly, the deterioration of battery lifetime affects the SoC estimation. Besides, the efficiency is usually determined by experiments, which makes calibration necessary.

5.2. Cell balancing

Due to the different capacities of battery cells caused by aging, use, manufacturing conditions, and so forth, cell balancing is needed to ensure that each battery cell is operating within its safety limits. The cell with the highest voltage will limit the amount of rechargeable electrical energy during charging, and thus limit the overall capacity of the battery pack. On the other hand, the cell with the lowest

voltage limits the amount of dischargeable electrical energy, as discharging will stop before the rest of the battery cells are at the discharge limit [49]. Figure 5.1 shows this limitation for charging and discharging (note that the configuration shown is not the battery configuration used).

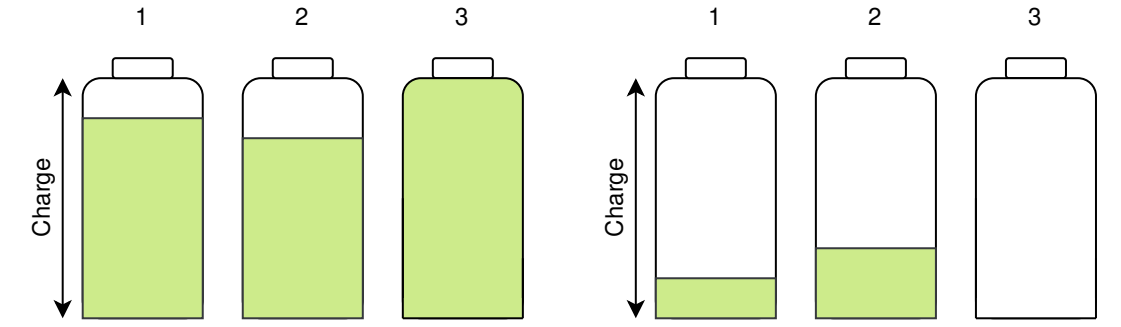

(a) Charging stops when the lowest capacity cell reaches full SoC, even though the other cells are not full yet.

(b) Discharging stops when the lowest capacity cell reaches zero SoC, even though the other cells still have charge left.

Figure 5.1: Cell imbalance during charging and discharging.

In a parallel configuration, balancing will already happen naturally, as the voltage across each cell will have to be equal, although extra balancing measures are often still implemented to ensure that the balancing currents do not exceed the maximum charging current of the cell, and that SoC is balanced as well [50]. In a series configuration, this does not happen automatically and thus always requires balancing circuitry [51].

5.2.1. Balancing methods

Two types of cell balancing methods exist: passive balancing and active balancing [52]. These two types will be elaborated further in the following two sections.

Passive balancing For passive balancing the extra energy from the most charged battery cells is dissipated in a resistor and thus lost. It is not transferred over to another cell. Furthermore, since the cell with the lowest capacity is the limiting factor during discharge and is not being recharged by the other cells, the total capacity of the battery pack is not increased over the weakest cell. Figure 5.2 shows this limitation during discharge.

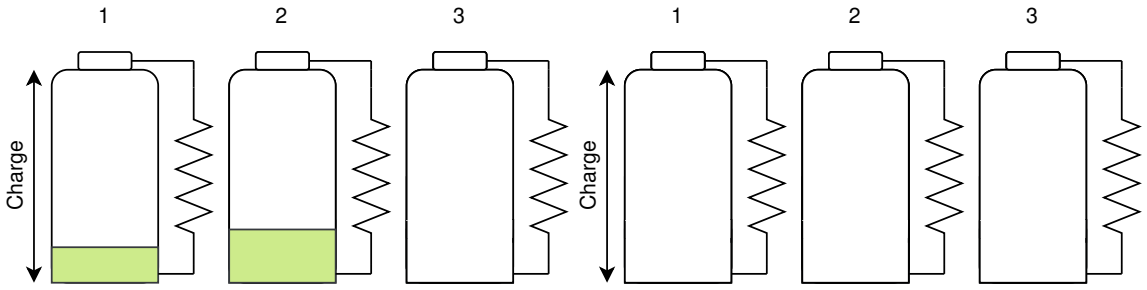

(a) Cell 3 has the lowest SoC, and the passive balancing circuitry discharges cell 1 and 2 via a resistor or transistor.

(b) Passive balancing finishes when all cells have been discharged. The discharged energy from cell 1 and 2 is not used for charging and is thus lost.

Figure 5.2: Passive balancing during discharge.

Passive balancing can be implemented by measuring individual cell voltage and SoC. Depending on the values of parameters, a switch can be turned on to connect the cell to a bleeding resistor. This way the cell discharges until it reaches the desired voltage and SoC again, and then the switch is turned off. This is the most often implemented balancing method in commercial ICs due to its easier control [53].

Active balancing Active balancing transfers extra energy from one cell to another. This way the energy is not dissipated and lost, as with passive balancing. Due to this, the total capacity of the battery

pack will be increased. During discharge, a cell with a higher SoC will charge the almost depleted cell, as shown in Figure 5.3.

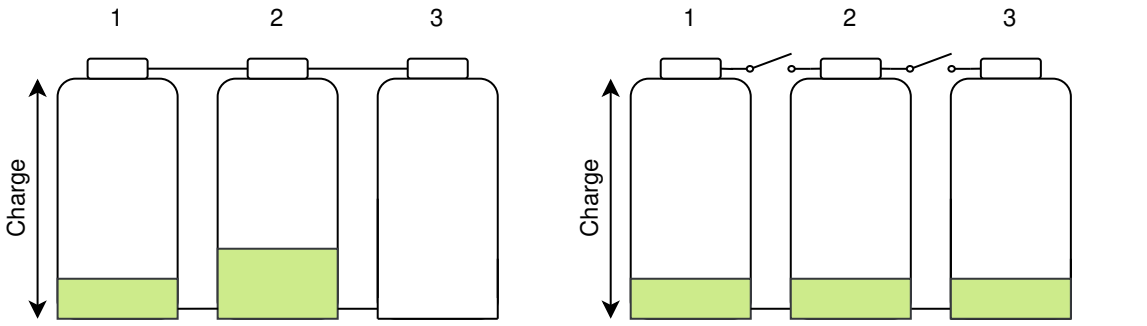

(a) Cell 3 reaches zero SoC first, and the active balancing circuitry charges cell 3 with cell 2.

(b) Active balancing is finished with all cells having the same voltage and SoC.

Figure 5.3: Active balancing during discharge.

Active balancing can be achieved via DC-DC converters or switched capacitors [54]. However, these only support energy transfer between adjacent cells and thus increases the total balancing time, and decrease the total efficiency. One possible method that does not have this limitation is the LC series circuit. Despite a higher efficiency, active balancing is not often used due to its added control complexity and costs.

5.3. Protection

Due to the volatility of the Li-ion battery [10, 55], protection circuitry is mandatory. Special care needs to be taken for overheating and overcharging (which results in overheating), as the liquid electrolyte is flammable [56].

5.3.1. Overcharge

Inherent to CC-CV charging is that the battery is already protected against overcharging. It will not go above the set upper voltage limit during charging. However, most of the time a separate form of overcharge protection is still built in. This is due to the fact that CC-CV only protects against overcharging if all cells are perfectly balanced. While this should be the case in correctly working systems, a fail-safe is often still used. Overcharge protection therefore will be based on each individual cell, instead of the total pack. The cell voltage of each battery cell will be measured individually and then compared to set limits. If it exceeds the threshold voltage, the charging circuit will be disabled. It will not re-enabled until the cell balancing circuit reduces the cell voltage below a certain release voltage again, which is set lower than the threshold voltage.

5.3.2. Overdischarge

Overdischarging of a battery cell causes its voltage to drop below its recommended operating range (i.e. undervoltage). This can cause permanent damage to it: the capacity will be reduced due to copper dissolution of the anode into the electrolyte and decomposition of the solid electrode interface, which results in the generation of gases [57]. Similar to overcharge protection, the cell voltage of each battery cell is measured individually and compared to set limits. When the set threshold values are reached, discharging is interrupted. A possible method to do this is via the use of a MOSFET that interrupts the power path from the battery to the load [58].

5.3.3. Overcurrent

Overcurrent or short-circuiting the battery, even if it is only momentarily, can cause damage to the battery, as it can drop the battery voltage below its safe threshold, causing the same problems as mentioned with overdischarge. Furthermore, a high current can cause excessive heat generation. To protect against this, a current-sense resistor can be used. The voltage across this resistor can then be measured and be compared to the set limits. Similar to overdischarge protection, the discharge path can then be interrupted to prevent further damage to the battery.

5.3.4. Temperature

Especially with Li-ion batteries, the operating temperature must be closely monitored. As is also explained in Section 3.1.3, operating under freezing temperature can cause permanent damage to the battery. On the other hand, operating above the recommended temperature limit (60 °C) can not only reduce the lifespan and efficiency of the battery but also cause internal sparks and ignite the liquid electrolyte [59]. To prevent this, thermal sensors should be implemented, so that the battery can be disconnected and shut down in time. Ideally, the internal temperature is measured of each cell individually. However, even though techniques have been demonstrated that can do this [60], most chips still use a combination of surface sensors and thermal models to estimate the internal temperature. Thin platinum resistive temperature devices that are less than 100 µm thick can be used to this end. In most cases, however, thermistors with a thickness in the range of 1 mm suffice [61].

5.4. Implementation

Different market available integrated circuits that implement cell balancing, SoC estimation, and various protection functions are presented in Table 5.1. Since all implementations support a wide range of protection features, this category is not considered during comparison.

Table 5.1: Selection of ICs on the market that support battery management functions.

Type	Series cells [cells]	SoC estimation	Balancing	Note	Cost [€/pc]
BQ40Z80	2–6	Coulomb & OCV	Passive	SoC display	4.76
BQ76942	3–10	Coulomb & OCV	Passive		4.29
BQ769142	3–14	Coulomb & OCV	Passive		4.52
BQ76952	3–16	Coulomb & OCV	Passive		4.76
LTC3300-1	2–6	None	Active	External voltage sensor	11.10
LTC3300-2	2–6	None	Active	External voltage sensor	10.66

Following from functional requirement [**F.6**], the SoC needs to be displayed, this can be done using the BQ40Z80. Due to trade-off requirement [**T.4**], the battery capacity should be as large as possible, an aspect that cell balancing helps with. The LTC3300 devices have a balancing efficiency of approximately 93 % [62, 63], which is evidently much higher than with passive balancing. On the other hand, it can be seen that the active balancing types are in the higher price range compared to passive balancing. Additionally, an external voltage sensor is needed for these types. Considering trade-off requirement [**T.2**], costs should be minimized. Considering all requirements, the BQ40Z80 is selected for battery management. The BQ40Z80 can be programmed via the SMBus protocol. The following paragraphs explain the specific implementation for SoC estimation, balancing, protection, and control using the BQ40Z80 [64, 65].

SoC estimation SoC estimations with the Impedance Track™ algorithm are supported. This algorithm includes both the voltage readout and coulomb counting method. When the battery is not supplying or charging (relaxed state), the SoC is calculated using the OCV-SoC curve. This is done for each separate cell and specific for the selected cell chemistry. In case the battery is in supplying or charging modes, the SoC is updated with the coulomb counting method. A temperature model with temperature prediction is included to increase the accuracy of the estimations.

In case a high to low transition is detected at the $\overline{\text{DISP}}$ pin, status information is shown on the LED display for a pre-defined time interval. The SoC can be selected on this LED display, in order to meet functional requirement [**F.6**]. All six LEDs can be set to a specific SoC threshold, where they start blinking or lighten solid. The circuit implementation can be seen in Appendix E.8.

Balancing Passive cell balancing is supported by the BQ40Z80. Dissipation resistors are connected in parallel to the individual cells. The balancing current is controlled by FETs in series with those resistors. Multiple cells can be balanced simultaneously with a maximum balancing current of 10 mA. External resistors can be used for higher balancing currents.

Cell balancing is possible during charging mode and relaxed mode. For the first, coulomb counting is used for SoC estimations. For the latter, OCV measurements are performed in order to calculate the charge difference between cells. Here, the temperature is also taken into account. The balancing time for specific cells determines how long the FET should be conducting by pulsing it with a pre-defined duty cycle. Balancing time is calculated based on the cell properties, series resistance, and FET resistance. The balancing circuit implementation is shown in Appendix E.8.

Protection The most important protection features, as mentioned in Section 5.3, are supported. Overcharge protection is included and extended into overcharging voltage and current protection. When the measured charging voltage is bigger than the programmed charging voltage, charging is terminated. The same action is executed when the actual charging current is measured to be higher than the programmed charging current. When the battery capacity is charged over its specified maximum capacity, charging is also terminated.

Overdischarge protection is integrated and listed as cell undervoltage- and overcurrent in discharge protection. First, cell undervoltage protection detects if individual cells are discharged too much and prevents them from becoming damaged. Overcurrent in discharge protection takes care that the discharging current stays below the programmed value.

Current protection is classified into overcurrent- and short-circuit protection. Overcurrent protection can be set with specific thresholds during charging and discharging. This is favorable since the battery specifies different maximum currents for these modes [24]. Short circuit protection is featured for both charging and discharging actions.

Individual cell temperature sensors can be connected in order to protect the cells against overtemperature and discharging below the minimum battery cell temperature. Protection processes disconnect the battery in case a temperature outside the allowed range is measured.

Control As mentioned in Section 4.1.3, the selected USB-PD controller has some side functions. This controller can be used to control the BQ40Z80. The main functions that need to be driven are the $\overline{\text{DISP}}$ pin for SoC display and status updates via the SMBus protocol. Besides, this controller can be used to switch off the charger when the end current of 175 mA has been reached, as specified in Section 4.4.1.

A push-button on the outside of the Wireless Powerlizer can be connected to the STM32L5x2 GPIO pins so that the user can decide when the SoC needs to be displayed. Two data pins of the controller can be connected to the SMBC and SMBD pins of the BQ40Z80 for the SMBus protocol. This protocol can be used to exchange status information. The $\overline{\text{VMODE}}$ pin of the LT3956 needs to be connected to a voltage sense pin of the controller. When $\overline{\text{VMODE}}$ is low, and the battery current is below 175 mA, one of the STM32L5x2 GPIO pins needs to disable an NMOS transistor in series with LT3956 pin EN/UVLO and ground to disable the charger. When one of these conditions is no longer met, the charger needs to be enabled again. The state diagram for the controller is shown in Figure 5.4.

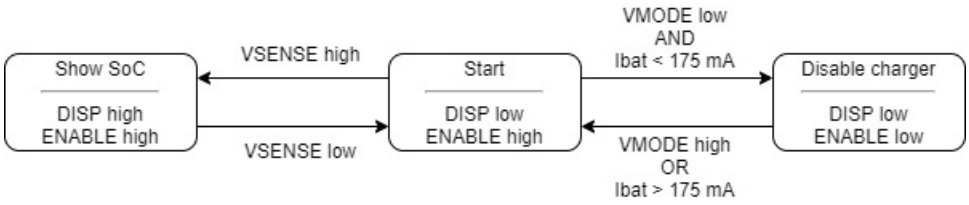

Figure 5.4: State diagram of the external controller.

5.5. Protection and balancing flowcharts

The simplified operating mechanism and algorithm of each protection and balancing feature can be summarized into a flowchart. For a more comprehensive description, the technical reference of the BQ40Z80 can be consulted.

Balancing As explained in Section 5.4, the BQ40Z80 uses parallel dissipation resistors and MOSFETs to balance each individual battery cell. Each cell will be discharged through this resistor until they reach the SoC of the weakest cell. In reality, a margin (e.g. 5 %) should be taken for the comparison with the lowest SoC, as otherwise it can potentially discharge to zero SoC when a cell is discharged below the former lowest SoC. The algorithm for each cell is shown in Figure 5.5.

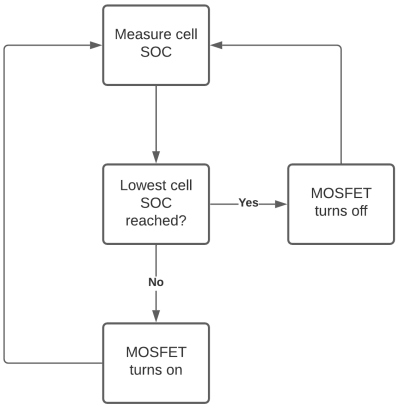

Figure 5.5: The cell balancing algorithm.

Protection The overcharge, overdischarge, and temperature protection all work similarly: the voltage and temperature are monitored, and charging or discharging is terminated when these parameters exceed the set thresholds. Charging or discharging is only resumed when these parameters have returned to the range of the release thresholds. Overcurrent protection on the other hand cannot continuously measure current as it disrupts the power path when triggered and hence will resume operation after a certain amount of time has passed (which is defined by the user) instead of having a release threshold. After five consecutive overcurrent fails (definable by the user), the overcurrent protection triggers indefinitely, until it is manually reset (e.g. with a button press or signal from the external MCU). Figure 5.6 shows the two general algorithms in a flowchart.

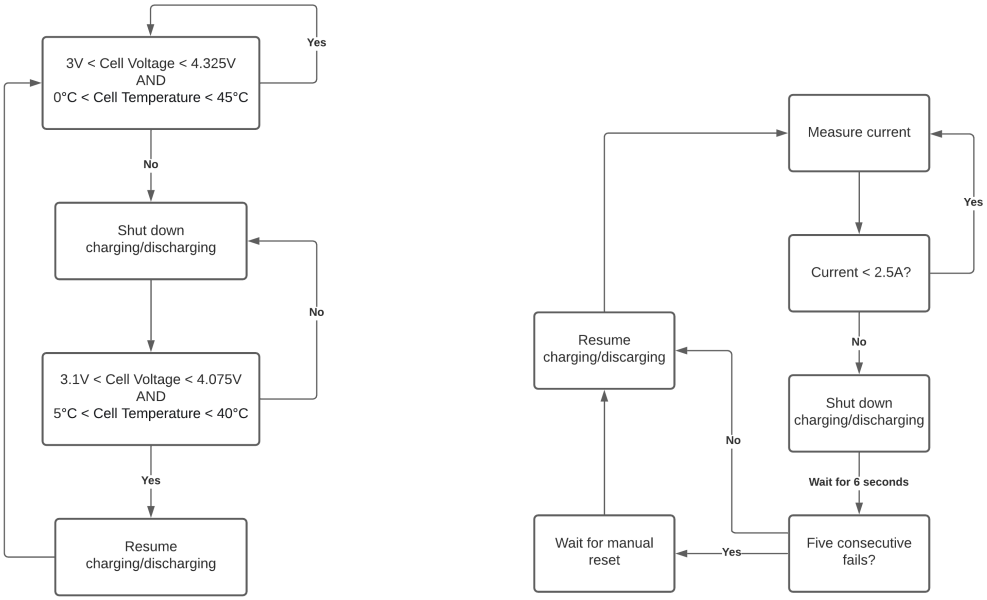

(a) The voltage and temperature protection algorithm.

(b) The current protection algorithm.

Figure 5.6: The algorithm for voltage, temperature, and current protection.

5.6. Simulation

The cell balancing method and the protection algorithms, as described in Section 5.5, have been implemented in Simulink using the charger and battery model of Section 4.5.1. The results and setup of these simulations will be discussed in this section.

5.6.1. Cell balancing

Cell balancing is achieved by connecting a MOSFET and resistor in parallel to each battery cell. The control of the MOSFET can be implemented via a MATLAB Function block. This block receives the SoC of each cell and determines which cell has the lowest SoC. Every cell that is above this SoC will have its parallel MOSFET turned on, and thus will start discharging. The schematic and code for the function block can be found in Appendix D.1. Figure 5.7 shows the balancing simulation: both when the battery is being charged and when the battery is at rest.

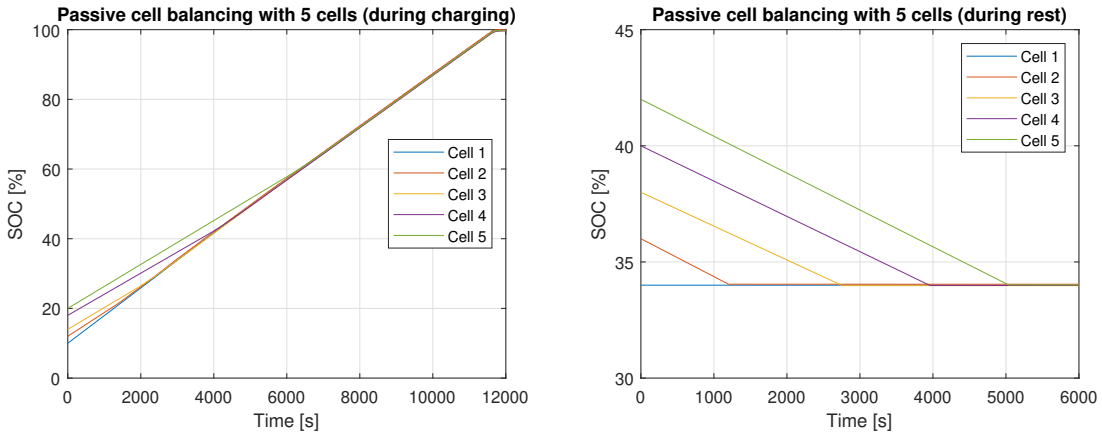

(a) Balancing during charging.

(b) Balancing during rest.

Figure 5.7: Cell balancing during rest and during charging. Each cell has a different initial SoC and different capacity.

5.6.2. Protection

Battery protection is achieved through a MATLAB Function block (similar to balancing). Depending on the input (e.g. cell voltage, battery current, etc.) it can pull low or pull high a MOSFET that disconnects or reconnects the battery to the charging circuit or load. The schematic and code for the function block can be found in Appendix D.2. Figure 5.8 shows the simulation results for each of the four algorithms mentioned in Section 5.5.

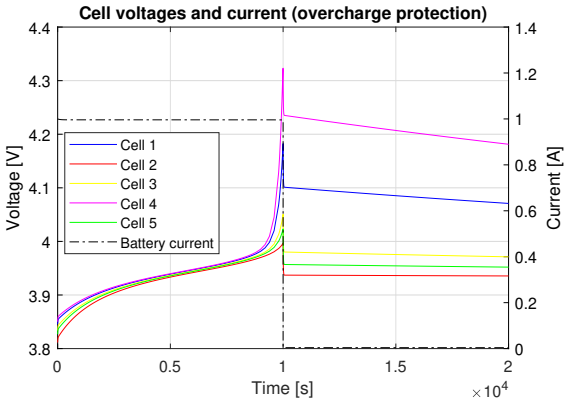

(a) Overcharge protection, triggered at 4.325 V.

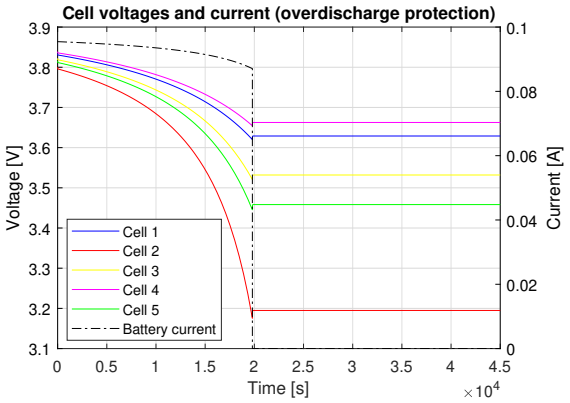

(b) Overdischarge protection, triggered at 3.2 V. Note that this is not 3 V, due to the battery model having a minimum voltage of 3.2 V.

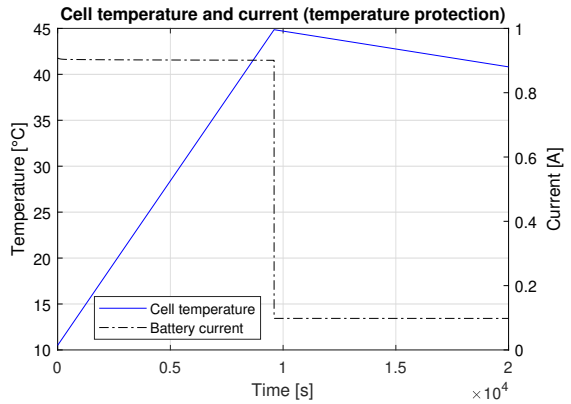

(c) Temperature protection, triggered at 45 °C.

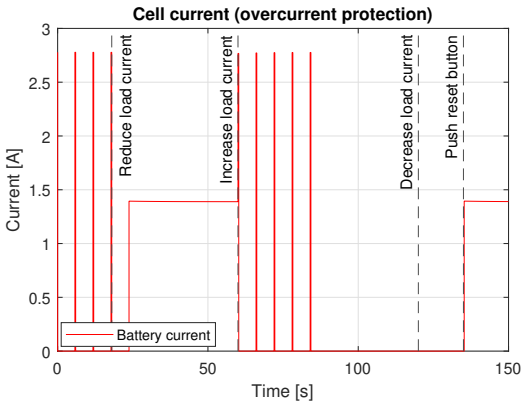

(d) Overcurrent protection, triggered at 2.5 A, with a reset timer of 6 s. Load current is varied over time. Manual reset required after five consecutive fails.

Figure 5.8: Different protection modules triggering in Simulink.

6 Prototype

The physical prototype is explained in this chapter. First, the scope of the prototype is discussed and the specific subsystems implemented in the prototype are chosen. Then, the design of the prototype is summarized. Finally, the prototype is verified by tests.

6.1. Scope

In order to verify the functionality of the battery management system, a prototype needs to be built. Limitations on time and budget make it unrealistic to test the whole system. The prototype implementation of the battery cell, battery charger, and battery management will be further outlined in the next paragraphs.

Battery cell A battery pack would help to show the charging behavior of the charger. However, there is no additional value in showing that the selected battery cell is able to discharge. In order to be able to safely charge batteries, a battery management system needs to be implemented as well. The combination of these two parts would be too expensive (and require too much time debugging) for its added value. Therefore, it will not be incorporated into the prototype. For the other subsystems, the battery will be mimicked by another component, such as a power supply.

Battery charger The battery charger consists of the USB controller and the converter with its control circuitry. Since the focus of the thesis is on power electronics, the USB controller will not be implemented in the prototype. Additionally, it holds less educational value to show that the purchased controller is functioning as described by the manufacturer.

The converter with its control circuit will be implemented in the prototype. For the input, a power supply with current regulation capabilities can be used to mimic the behavior of the USB-C input. For the output, a power supply in parallel with a power resistor can be used to mimic the behavior of the battery cells. As the battery voltage needs to increase during charging, when the converter is still in constant current mode, the voltage over the resistor needs to be set by a power supply.

Battery management For the battery management system, a prototype will not be made. As mentioned before, the battery management system is too expensive and its costs cannot be justified for its added value (especially since it will not be used by others after this project). Additionally, it is not actually required, since no batteries are being used. Also, similar to the USB controller, the chip is a complete stand-alone circuit, such that it virtually is a black box and does not provide additional insight into the functionality of the protection features.

6.2. Design

A prototype of the battery charger has been made as PCB since the LT3956 IC is only available as an SMD component. KiCad has been used for PCB design. The schematic and layer prints are depicted in Appendix E.1. Figure 6.1 shows a render of the PCB.

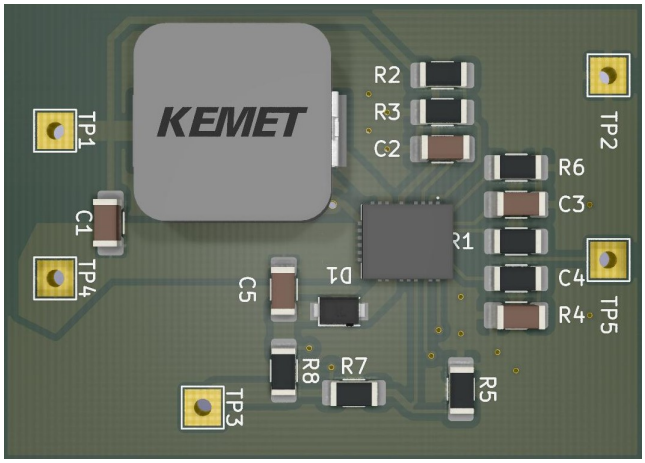

Figure 6.1: Render of the prototype PCB.

Since one of the resistors in the feedback loop (see Section 4.4.3 for the setup) was not delivered, an available replacement resistor of 150 kΩ was used. This gives a CV-mode voltage of 20 V. Since no real battery will be used for the prototype, this will not present problems.

6.3. Verification

The verification of the prototype will be done according to the test plan shown in Appendix F. These tests are classified into startup behavior, CC-mode behavior, CV-mode behavior, thermal behavior, and mode-switching behavior. An input power supply with a current limit is needed to mimic the USB input. For the output, a variable power resistor is needed to mimic the behavior of the battery.

The results of the startup, thermal, CC-, and CV-mode tests are presented in the following sections. The mode switching test is presented in Appendix C.1.

6.3.1. Startup

The result for the startup test with an 18 Ω load resistor can be seen in Figure 6.2.

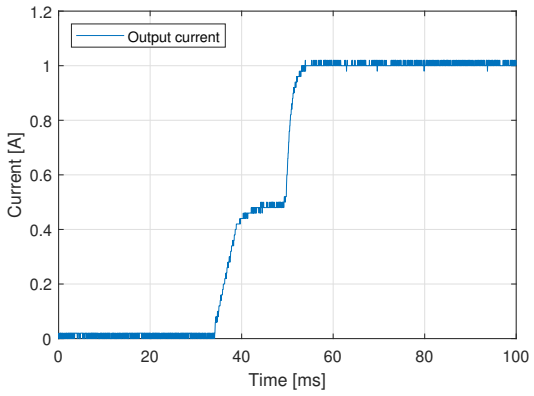

Figure 6.2: Output current during startup.

The output current first increases to 0.5 A. This is the current needed to bring the output voltage to the input voltage level, which is 9 V. The step results from the use of a resistor to mimic the battery behavior. After this, soft-start appears to be enabled and brings the output current to the wanted 1 A in roughly 2 ms, which is the soft-start time that was calculated. In Table 6.1, the current during the first step in the startup is shown, where it can be seen that the current indeed decreases as resistance increases. Appendix C.2 shows the startup behavior with a load resistance of 15 Ω graphically.

Table 6.1: Output current step measured during startup with different load resistances.

Resistance [Ω]	Step current [mA]
15.0	552
16.0	528
17.0	496
18.0	472

6.3.2. CC-mode

The results of the tests performed in CC-mode can be found in Table 6.2. It can be seen that the output current stays constant at 1 A, regardless of load resistance (as long as output voltage does not exceed the CV threshold).

The inductor current ripple was measured to be 300 mA, which is higher than the simulated 226 mA, which can be explained by the 20 % tolerance of the inductance and the DC bias. The DC bias reduces the effective inductance, and hence increases the current ripple. It still is lower than the maximum allowed ripple of 816.6 mA.

The output voltage ripple during CC-mode can also be seen to be below the maximum allowed value. ΔV_{out} remains below the maximum 1.25 V, and aligns reasonably well with the theoretical value of 1 V, when taking into account possible capacitance variations. The difference in output voltage ripple between the different load resistances can again be explained by the DC bias. In the same manner as with the inductor, a higher DC voltage over the capacitor decreases the effective capacitance, thereby increasing voltage ripple.

The measured efficiency during CC-mode was 92.0 % (measured at R_{load} of 17.5 Ω, which aligns with the efficiency found in the LTspice simulation of 92.8 %).

6.3.3. CV-mode

The results of the tests performed during CV-mode can be found in Table 6.3. The output voltage is held reasonably constant around 19.5 V. This is lower than the expected 20 V. This difference is due to the tolerance of the resistances used, as a 2.67 % reduction of the 150 kΩ resistor will indeed result in a constant voltage of 19.5 V. Furthermore, the output current also logically decreases as resistance increases.

The output current ripple is well below the maximum allowed value of 350 mA, and thus should not present issues with the end-current. The output voltage ripple slightly exceeds the maximum allowed value. This is, similar to CC-mode, due to the decreased effective capacitance at higher DC voltages. To solve this, a larger capacitance should be chosen such that even with DC bias, temperature-dependent variations, and tolerance it is above the minimum capacitance of 2.2 µF.

The measured efficiency at a load resistance of 24.5 Ω is 93.6 %. This is in line with the simulated 94 %.

Table 6.2: Measurement on output during CC mode.

R_{load} [Ω]	I_{out} [mA]	V_{out} [V]	ΔV_{out} [V]
15	994	14.9	0.88
16	998	15.8	0.88
17	997	16.8	1.12
18	997	17.8	1.12

Table 6.3: Measurement on output during CV mode.

R_{load} [Ω]	I_{out} [mA]	ΔI_{out} [mA]	V_{out} [V]	ΔV_{out} [V]
20	997	19.2	19.4	1.20
21	931	19.2	19.5	1.20
22	902	17.6	19.6	1.28
23	854	17.6	19.6	1.28

The inductor current ripple is presented in Figure 6.3 and was measured to be 380 mA. This exceeds the simulated 270 mA current ripple, but it can be seen that it increases when compared to CC-mode, which coincides with the simulations.

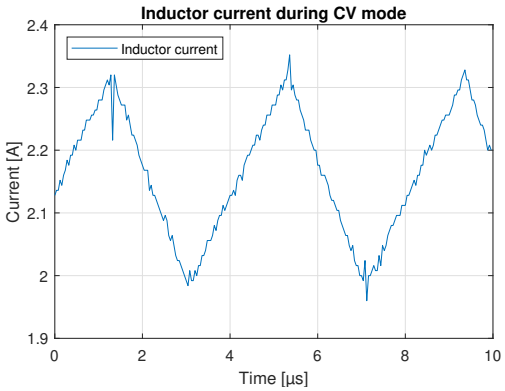

Figure 6.3: The inductor current measured in CV mode.

During both CC- and CV-mode tests, the switching frequency was measured to be 263 kHz, which is consistent with the simulated 259.2 kHz.

Thermal The result of the thermal test is presented in Figure 6.4. Here, the ambient temperature was approximately 21 °C. The overlay is slightly misaligned vertically. The highest temperature is measured around the diode and the IC, which aligns with the expectations. The measured 41.9 °C is lower than the theoretical values estimated in Section 4.6. This is partly due to the resolution of the thermal camera, as it may not be able to precisely measure the temperature of the diode or IC. Furthermore, the theoretical values were obtained using the maximum junction-to-ambient thermal resistance, which is usually higher than the actual package thermal resistance.

Figure 6.4: Thermal image of the prototype.

7

Conclusion and Recommendations

This chapter describes the conclusions that can be drawn from this thesis. After that, recommendations are given for future work.

7.1. Conclusion

This thesis discussed the design decisions made regarding the batteries and battery management system for the Wireless Powerlizer. The battery cell and its configuration were selected in Chapter 3 such that functional requirements [**F.2**], [**F.3**], and [**F.4**] are met. Li-ion was chosen as chemistry in order to meet trade-off requirements [**T.4**] and [**T.2**]. It was outlined that it has the highest performance based on volumetric energy density and specific energy. The configuration was selected as 5S1P such that it is capable of providing at least 2 full phone charges for wireless charging with an estimated worst-case 50 % efficiency and enough energy for disinfection. With this battery chemistry and configuration, it is also possible to deliver the required 34 W when taking the efficiency for the UV-C and wireless charging modules into account.

In Chapter 4, the charging method was selected as CC-CV in order to meet trade-off requirement [**T.5**]. This method is able to charge the chosen battery as fast as possible while also taking safety into consideration (requirement [**S.1**]. The designed converter was a DC-DC boost converter with current and voltage feedback. First, the overall charging control was simulated using Simulink. Then, the LT3956 was selected as controller for the converter. The final design was simulated in LTspice and showed that it behaves as desired.

Then, in Chapter 5 the battery management module is elucidated. This entails the choice of the USB-PD controller, the battery management chip BQ40Z80, and it describes the required balancing and protection features for the battery pack. The general workings of the protection algorithms and the cell balancing algorithm are also described and simulated in Simulink, which showed the expected results, and thus meets requirement [**S.1**]. The high-level controller is also described, which is used to set an end-current for charging and can control the LEDs to indicate status, satisfying requirement [**F.6**].

A prototype for the battery charger was presented and verified in Chapter 6. Testing of the PCB showed that it meets all but one requirement of the performed tests: the output voltage ripple was too high, which is to be solved by increasing the output capacitance. Charging control was also shown to be functioning correctly, which helps meet requirement [**T.5**].

7.2. Recommendations

Although this thesis captured a significant part of the design of the battery management system, there were still some things not possible in the time span of the project. Furthermore, there are some points of improvement that can be implemented for better overall performance.

USB-C input Currently, the tests are performed with a power supply as input source. Ideally, the USB-C connection and USB-PD protocol would also be included in the tests. While an IC has been chosen that, in theory, should be able to handle this, tests should be performed to confirm this. Furthermore, the

USB-PD protocol can support higher power draws than the system was designed for, and to increase charging speed (as per requirement [**T.5**]), this possibility should be taken advantage of.

High-level controller A global, high-level controller that controls the visible display on the Powerlizer is also not tested in this thesis. Since this controller should also control the end-current of the charger, this should be tested in conjunction with the battery charger circuit, ideally on one single PCB. This high-level controller must also be supplied with power, and most likely will require a buck converter to be designed.

Battery charger improvements In our current version of the battery charger, an asynchronous boost converter is used. However, testing shows that due to the large current (1 A average), the diode causes a lot of conduction loss. A synchronous boost converter would reduce losses in this case, as the MOSFET has a lower drain-source voltage and thus lower conduction losses. On the other hand, this does mean that the boost regulator must also support this synchronous design, and that switching losses will increase. However, since the switching frequency is relatively low (250 kHz), the overall losses will decrease.

Battery charger testing For the next version of the prototype, more extensive testing should be done. The battery has been mimicked by a power resistor instead of a real battery pack. The power resistor can represent the behavior of the battery, but ultimately is a simplified model: it does not simulate the capacitive effects of the battery, nor does it simulate the SoC.

Safety During the design of the battery management system, some parts of the IEC 62113:2017 were incorporated from the available summaries. However, because the availability of the standard is restricted, it could not be investigated in detail for this project. Although the design was made as safe as possible, in further designs and prototypes, the safety standard should be consulted and have its requirements incorporated.

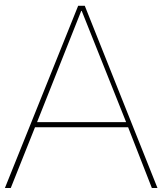

Abbreviations

Abbreviation	Description
BMS	Battery management system
CC	Constant current
CV	Constant voltage
CCM	Continuous conduction mode
COVID-19	Coronavirus disease 2019 (SARS-CoV-2)
DC	Direct current
DCM	Discontinuous conduction mode
DFP	Downstream facing port
DRD	Dual role data
DRP	Dual role power
EN	Enable
ESR	Equivalent series resistance
IC	Integrated circuit
IEC	International electrotechnical commission
LED	Light-emitting diode
Li-ion	Lithium-ion
MOSFET	Metal–oxide–semiconductor field-effect transistor
MCU	Microcontroller unit
OCV	Open circuit voltage
Pb-acid	Lead-acid
PCB	Printed circuit board
PI	Proportional–integral [controller]
PWM	Pulse-width modulation
RX	Receive
SBU	Side band use
SEPIC	Single ended primary inductor converter
SMBus	System management bus
SoC	State of charge
TX	Transmit
UFP	Upstream facing port
USB	Universal serial bus
USB BC	Universal serial bus battery charging
USB-PD	Universal serial bus power delivery
UV	Ultraviolet
UVLO	Under voltage lock out
WCS	Wireless charging system

B

Elaborations

B.1. Battery cell

This appendix contains the chemical reactions during charging and discharging for the discussed battery cell chemistries.

Lead-acid Lead reacts with hydrogen-sulfate to form two electrons at the negative electrode during discharging. This process is reversed during charging as shown in B.1.

$$\mathrm{Pb} + \mathrm{HSO_4^-} \underset{\text{charge}}{\overset{\text{discharge}}{\rightleftharpoons}} \mathrm{PbSO_4} + \mathrm{H^+} + 2\,\mathrm{e^-} \tag{B.1}$$

Two electrons react with lead-oxide and hydrogen-sulfate at the positive electrode to form lead-sulfate and water during discharging. This process is reversed during charging as shown in B.2

$$\mathrm{PbO_2} + \mathrm{HSO_4^-} + 3\,\mathrm{H^+} + 2\,\mathrm{e^-} \underset{\text{charge}}{\overset{\text{discharge}}{\rightleftharpoons}} \mathrm{PbSO_4} + 2\,\mathrm{H_2O} \tag{B.2}$$

Nickel-metal hydride Metal Hydride reacts with hydrooxide-ions to form water, a metal, and an electron at the negative electrode during discharging. This process is reversed during charging as shown in B.3

$$\mathrm{MH} + \mathrm{OH^-} \underset{\text{charge}}{\overset{\text{discharge}}{\rightleftharpoons}} \mathrm{M} + \mathrm{H_2O} + \mathrm{e^-} \tag{B.3}$$

An electron reacts with water and nickel oxyhydroxide to form nickel hydroxide and a hydroxide-ion at the positive electrode during discharging. This process is reversed during charging as shown in B.4

$$\mathrm{NiOOH} + \mathrm{H_2O} + \mathrm{e^-} \underset{\text{charge}}{\overset{\text{discharge}}{\rightleftharpoons}} \mathrm{Ni[OH]_2} + \mathrm{OH^-} \tag{B.4}$$

Li-ion Li-ions in both the oxidation reactions move through the electrolyte. For a cobalt-oxide Li-ion battery, lithium-carbide forms graphite, a Li-ion and an electron at the negative electrode during discharging. This process is reversed during charging as shown in B.5

$$\mathrm{C_6Li} \underset{\text{charge}}{\overset{\text{discharge}}{\rightleftharpoons}} 6\,\mathrm{C} + \mathrm{Li^+} + \mathrm{e^-} \tag{B.5}$$

Cobalt oxide reacts with a Li-ion and an electron at the positive electrode to form lithium-cobalt-oxide during discharging. This process is reversed during charging as shown in B.6

$$\mathrm{CoO_2} + \mathrm{Li^+} + \mathrm{e^-} \underset{\text{charge}}{\overset{\text{discharge}}{\rightleftharpoons}} \mathrm{LiCoO_2} \tag{B.6}$$

B.2. USB Profile description

This appendix contains descriptions for the discussed USB profiles.

USB 2.0 As specified in the USB 2.0 standard [19], a device can draw up to 500 mA. A device can be a low-power or high-power device. In order to draw power, a controller is required. The maximum current that can be drawn per device class is expressed in unit loads. One unit load is equal to 100 mA. Low-power devices may draw a maximum of one unit load from the cable when operational, where high-power devices may draw between 1 and 5 units loads from the cable when fully powered. The USB 2.0 standard enables power transfer over either the low-power-port with voltage in range 4.40–5.5 V and current 100 mA, or the high-power-port with voltage in range 4.75–5.5 V and current 500 mA. A pull-down resistor of 14.25–15.75 kΩ shall be placed between each of *D+* and *D-* line and GND. A decoupling capacitor with value 1.0–10.0 µF shall be placed between *Vbus* and *GND*.

USB 3.x The USB 3.1 standard specifies one unit load as 150 mA and allows high-power-devices to draw a maximum of 6 unit loads. In order to draw power, a controller is required. The standard has equal voltage boundaries for both low-power-port and high-power-port, ranging 4.45–5.5 V. The allowed current draw equals 150 mA for the low-power-port and 900 mA for the high-power-port [23]. The USB 3.2 standard [21] sets a distinction between single-lane and multi-lane devices. The voltage for both low-power port and high-power port ranges 4.75–5.5 V. For the low-power port, the allowed current draw equals 150 mA for single-lane and 250 mA for multi-lane. For the high-power port, allowed current draw equals 900 mA for single-lane and 1500 mA for multi-lane. A dedicated controller is required to implement charging with USB 3.x standards.

USB BC 1.2 For USB Battery Charge (BC) v1.2, there are three port configurations possible: standard downstream port (SDP), dedicated charging port (DCP), and charging downstream port (CDP) [20]. Downstream ports are end-devices whereas upstream ports are seen as hosts. First, a SDP could be a host or hub complying with USB 2.0. It expects a current draw of 2.5 mA, up-to 100 mA, or up-to 500 mA depending on the configuration. For configuring as SDP, both *D+* and *D-* pins shall be pulled down to ground through two 15 Ω typically resistors. The port defines its current draw by sensing the *D+* line. Secondly, a DCP is a dedicated power output port. It is not capable of enumerating (detecting) a downstream device. A DCP requires a controller for detecting if a connection has been made. Lastly, a CDP is a downstream port that could be a host or hub complying with USB 2.0. A CDP shall sense the *D-* line and, if an upstream port is detected, output a voltage on the *D+* line.

Type-C 1.2 The USB-Type C 1.2 can draw currents equal to 1.5 A and 3 A [18]. Pull-down resistors of 5.1 kΩ $\pm$10 % shall be placed between ground and both *C1* and *C2* pins. Depending on the resistor values of the connected downstream facing port, the supply current is either 1.5 A or 3 A. The voltage on both the *C1* and *C2* pins pins shall be monitored to detect if an appropriate connection has been made. The voltage combination determines the maximum current that may be drawn by the port.

Power delivery The USB Power Delivery (PD) standard admits the biggest possible power draw. Negotiation between host and device occurs over the *CC* pins to establish the power transfer [22]. A controller is required for the communication. USB-PD allows multiple voltages with different power ranges. In case of 5 V, the maximum power transfer equals 15 W. Next is 9 V with power 15–27 W. Then, 20 V with possibility 45–60 W and 60–100 W.

B.3. LT3956 internal MOSFET losses

While there is no information about the switching losses and characteristics of the internal MOSFET for the LT3956, it does provide the on-resistance vs temperature in its datasheet, with which the conduction loss can be calculated. In the operating range from 0–125 °C (which is its maximum allowed temperature), it has an R_{on} of 80–165 mΩ, which is fairly high: other MOSFETs on the market (with the required voltage and current ratings) in the same temperature range can go as low as 0.9–1.7 mΩ.

With a nominal temperature of 25 °C, the difference is 90 mΩ against 1 mΩ (internal against external MOSFET). With an RMS current of 2.2 A, this leads to a conduction loss of 436 mW for the internal MOSFET, and a potential conduction loss of 5 mW for an external MOSFET.

C

Figures

C.1. Prototype mode switching

The prototype mode switching behavior is verified using the test shown in Figure C.1.

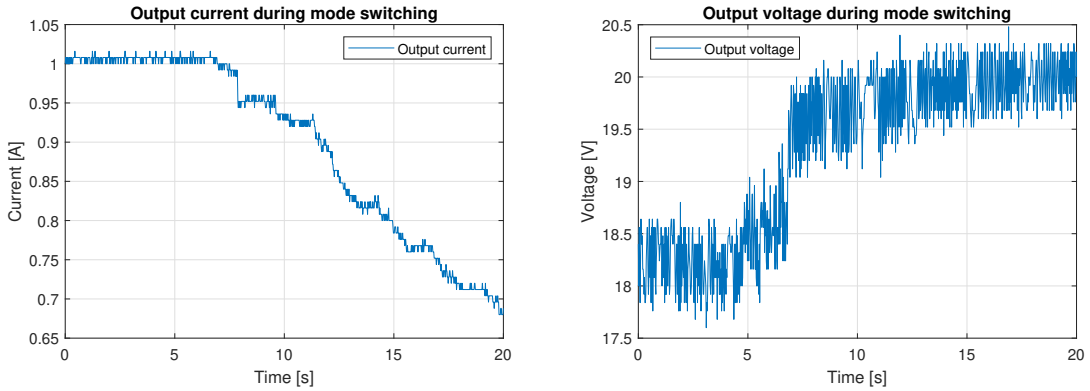

Figure C.1: The output current and voltage measured during switching from CC to CV mode.

C.2. Prototype startup

The prototype startup behavior test output current with different load resistances is shown in Figure C.2.

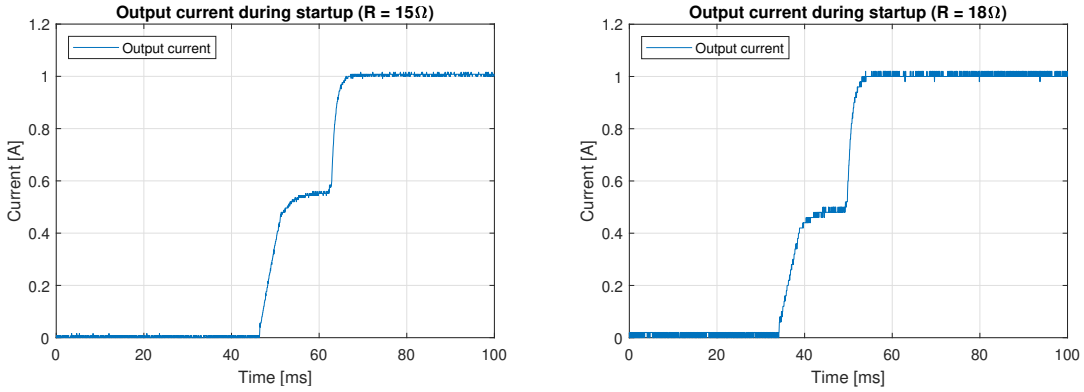

Figure C.2: The output current measured during startup with different load resistances.

D

Listings

This appendix contains all written software for the battery management simulations.

D.1. MATLAB Balancing control function block

```
%%%%%%%%%%%%%%%%%%%%%%%%%%%%%%%%%%%%%%%%%%%%%%%%%%%%%%%%%%%%%%%%%%%%%%%%%%%%
% Simulink balancing block                                                    %
% Authors: Jeroen van Ammers, Hsukang Chen                                    %
% -Inputs:                                                                    %
%   soc1-5 = Battery SOC of the five cells                                    %
%                                                                             %
% -Outputs:                                                                   %
%   gate1-5 = Gate of the MOSFET in the dissipation path of each cell%
%%%%%%%%%%%%%%%%%%%%%%%%%%%%%%%%%%%%%%%%%%%%%%%%%%%%%%%%%%%%%%%%%%%%%%%%%%%%
function [gate5, gate4, gate3, gate2, gate1] = balancing(soc5,soc4,soc3,
    soc2,soc1)

%Convert SOC reading to integer (can be int16, int32, or any integer)
y5 = int16(soc5);
y4 = int16(soc4);
y3 = int16(soc3);
y2 = int16(soc2);
y1 = int16(soc1);

%Determine lowest SOC
lowestSOC = min([y5 y4 y3 y2 y1]);

%Test each cell SOC to see if it is the lowest one in the pack
if(y5 == lowestSOC)
    gate5 = 0;
else
    gate5 = 1;
end

if(y4 == lowestSOC)
    gate4 = 0;
else
    gate4= 1;
end

if(y3 == lowestSOC)
```

```
    gate3 = 0;
else
    gate3 = 1;
end

if(y2 == lowestSOC)
    gate2 = 0;
else
    gate2 = 1;
end

if(y1 == lowestSOC)
    gate1 = 0;
else
    gate1 = 1;
end

end
```

D.2. MATLAB Protection function block

```
%%%%%%%%%%%%%%%%%%%%%%%%%%%%%%%%%%%%%%%%%%%%%%%%%%%%%%%%%%%%%%%%%%%%%%%%%%%%%%%
% Simulink protection block                                                    %
% Authors: Jeroen van Ammers, Hsukang Chen                                     %
% -Inputs:                                                                     %
%   batV1-5 = Battery voltage of the five cells                                %
%   batCurrent = Battery current                                               %
%   batTemp = Battery temperature                                              %
%   resetManual = Manual reset (for indefinite overcurrent failure)            %
%                                                                              %
% -Outputs:                                                                    %
%   ingateOut = Gate of the MOSFET in the charging path                        %
%   outgateOut = Gate of the MOSFET in the discharging path                    %
%%%%%%%%%%%%%%%%%%%%%%%%%%%%%%%%%%%%%%%%%%%%%%%%%%%%%%%%%%%%%%%%%%%%%%%%%%%%%%%
function [ingateOut, outgateOut, perm] = protection(batV1,batV2,batV3,
    batV4,batV5, batCurrent, batTemp, resetManual)
%These values have to carry over from call to call
persistent overVoltageActive
persistent underVoltageActive
persistent overCurrentActive
persistent tempActive
persistent ingate
persistent outgate
persistent timer
persistent permFail

%Initialize values
if isempty(overVoltageActive)
    overVoltageActive = 0;
    underVoltageActive = 0;
    overCurrentActive = 0;
    tempActive = 0;
    ingate = 1;
    outgate = 1;
    timer = 0;
```

```
34      permFail = 0;
35  end
36  on = 1;
37  off = 0;
38
39  batCurrent = abs(batCurrent); %Battery current can be negative
40
41  overvoltageTrigger = 4.325; %Triggers at 4.325V
42  overvoltageRelease = 4.075; %Releases at 4.075V
43
44  undervoltageTrigger = 3.2; %Ideally 3V, but Simulink battery model does
        not support it
45  undervoltageRelease = 3.3; %Releases at 3.3V
46
47  overcurrentTrigger = 2.5;  %Triggers at 2.5A
48
49  temperatureTrigger = 45;   %Triggers at 45 degrees Celsius
50  temperatureRelease = 40;   %Releases at 40 degrees Celsius
51
52  %Overcharge
53  %Check if any cell voltage is above the trigger point
54  if (batV1 > overvoltageTrigger || batV2 > overvoltageTrigger || batV3 >
        overvoltageTrigger || batV4 > overvoltageTrigger || batV5 >
        overvoltageTrigger)
55      ingate = off;
56      overVoltageActive = 1;
57  end
58
59  %If triggered, check if all the battery cells are below the release point
60  %before releasing
61  if (overVoltageActive == 1)
62      if (batV1 < overvoltageRelease && batV2 < overvoltageRelease && batV3
            < overvoltageRelease && batV4 < overvoltageRelease && batV5 <
            overvoltageRelease)
63          ingate = on;
64          overVoltageActive = 0;
65      end
66  end
67
68  %Overdischarge
69  %Check if any of the cells are below the trigger point
70  if (batV1 < undervoltageTrigger || batV2 < undervoltageTrigger || batV3 <
        undervoltageTrigger || batV4 < undervoltageTrigger || batV5 <
        undervoltageTrigger)
71      outgate = off;
72      underVoltageActive = 1;
73  end
74
75  %If triggered, release only when all cells are above release point
76  if (underVoltageActive == 1)
77      if (batV1 > undervoltageRelease && batV2 > undervoltageRelease &&
            batV3 > undervoltageRelease && batV4 > undervoltageRelease && batV5
             > undervoltageRelease)
78          outgate = on;
79          underVoltageActive = 0;
80      end
```

```
81  end
82
83  %Overcurrent
84  %Reset consecutive fail counter to 0 if it does not trigger straight away
85  if (permFail > 1 && overCurrentActive == 0 && ingate && outgate && timer
        == 0)
86      if batCurrent < overcurrentTrigger
87          permFail = 0;
88      end
89  end
90
91  %Check if the battery current is above the trigger point
92  if batCurrent > overcurrentTrigger
93      ingate = off;
94      outgate = off;
95      overCurrentActive = 1;
96      permFail = permFail + 1;        %Add one to the consecutive fail counter
97  end
98
99  %If five consecutive fails, wait until manual reset is high
100 if permFail > 4
101     ingate = off;
102     outgate = off;
103     overCurrentActive = 0;
104     if resetManual
105         permFail = 0;
106         ingate = on;
107         outgate = on;
108     end
109 end
110
111 %Wait for 6 seconds before releasing
112 if (overCurrentActive == 1)
113     timer = timer + 1;
114     if timer == 24
115         timer = 0;
116         ingate = on;
117         outgate = on;
118         overCurrentActive = 0;
119     end
120 end
121
122 %Temperature
123 %Check battery temperature
124 if batTemp > temperatureTrigger
125     ingate = off;
126     outgate = off;
127     tempActive = 1;
128 end
129
130 %Release if below release point
131 if (tempActive == 1)
132     if batTemp < temperatureRelease
133         ingate = on;
134         outgate = on;
135         tempActive = 0;
```

```
136     end
137 end
138
139 %Outputs
140 perm = permFail;
141 ingateOut = ingate;
142 outgateOut = outgate;
143 end
```

E

Schematics

This appendix contains the schematics for the simulations, chosen integrated circuits, and prototype.

E.1. Prototype schematic

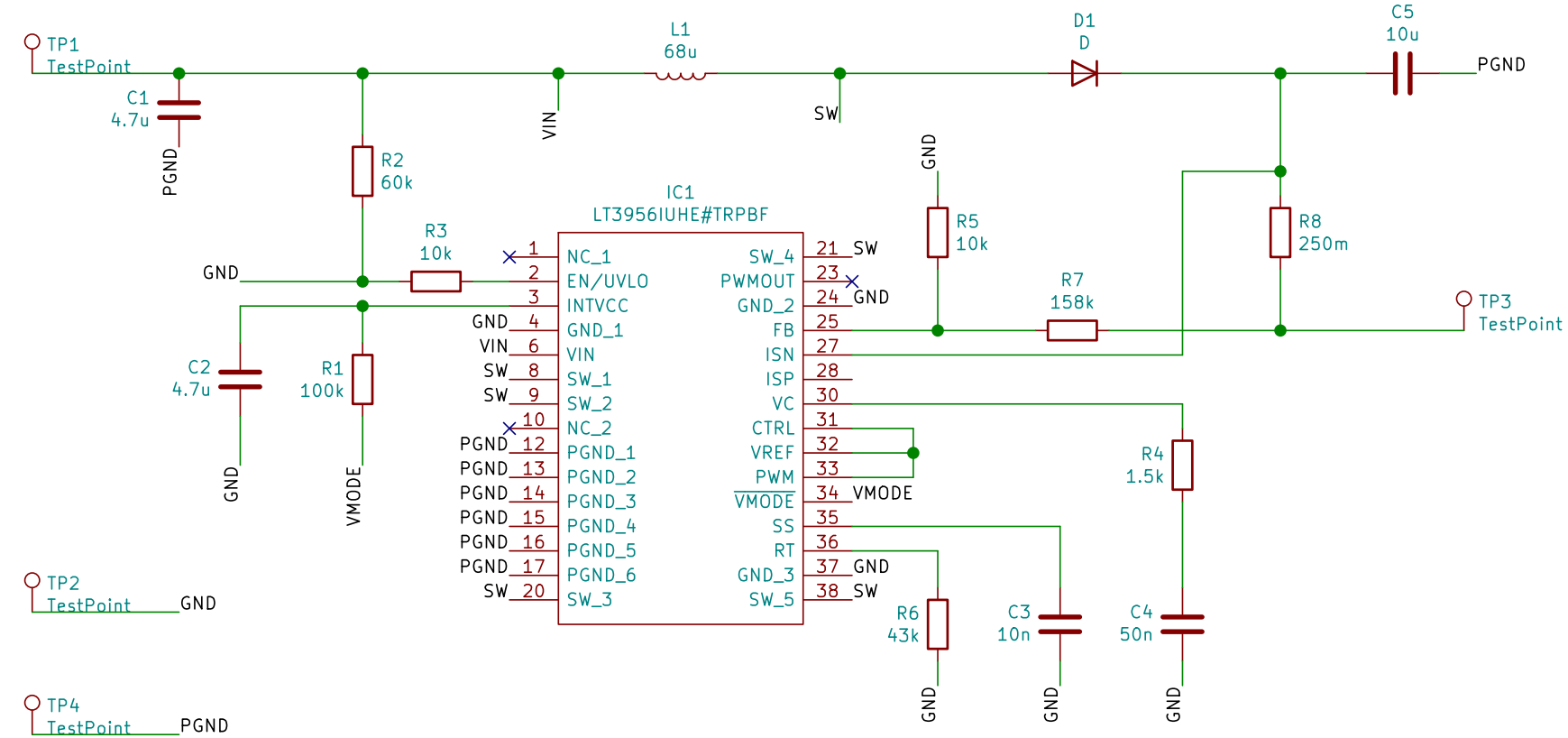

TU Delft

Sheet: /
File: BoostConverter.sch

Title: Battery Charger: Converter

Size: User	Date: 2021-06-05	**Rev: 1.0**
KiCad E.D.A. kicad (5.1.10)-1		Id: 1/1

E.2. Prototype board layout

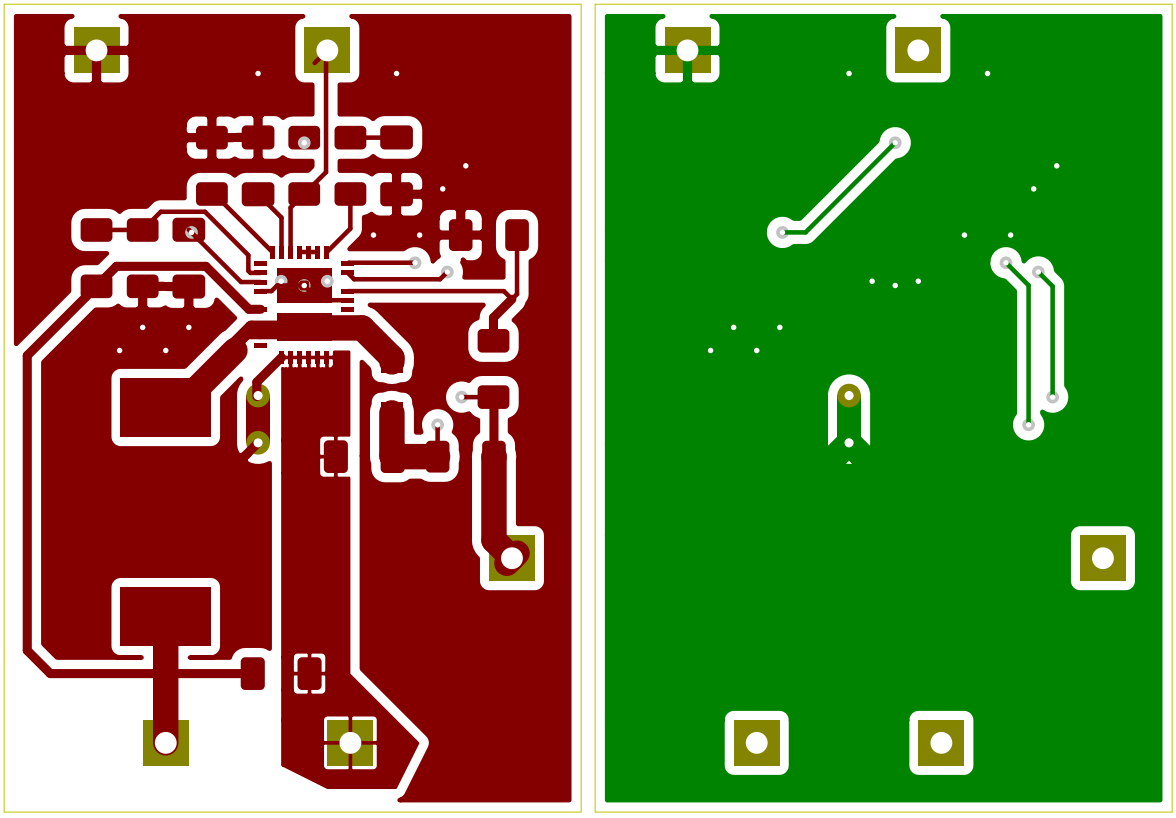

(a) Front (b) Back

Figure E.1: Prototype PCB Layout.

E.3. Simulink CC-CV charger

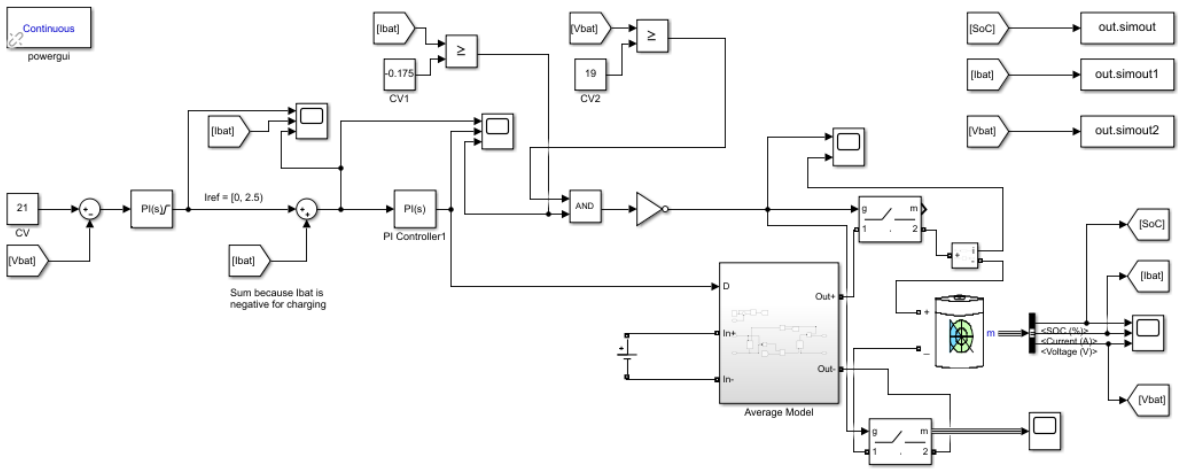

Figure E.2: Simulink simulation setup for CC-CV charging.

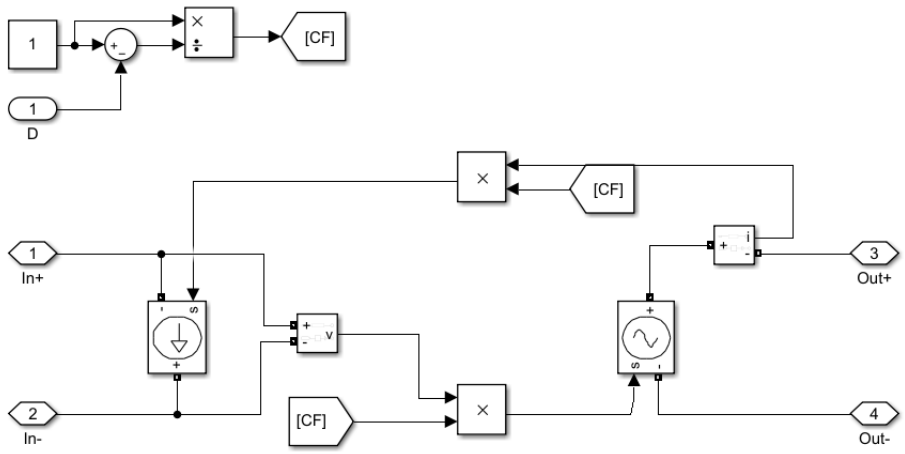

Figure E.3: Average boost converter model used in the CC-CV Simulink simulation.

E.4. LTspice CC-CV charger

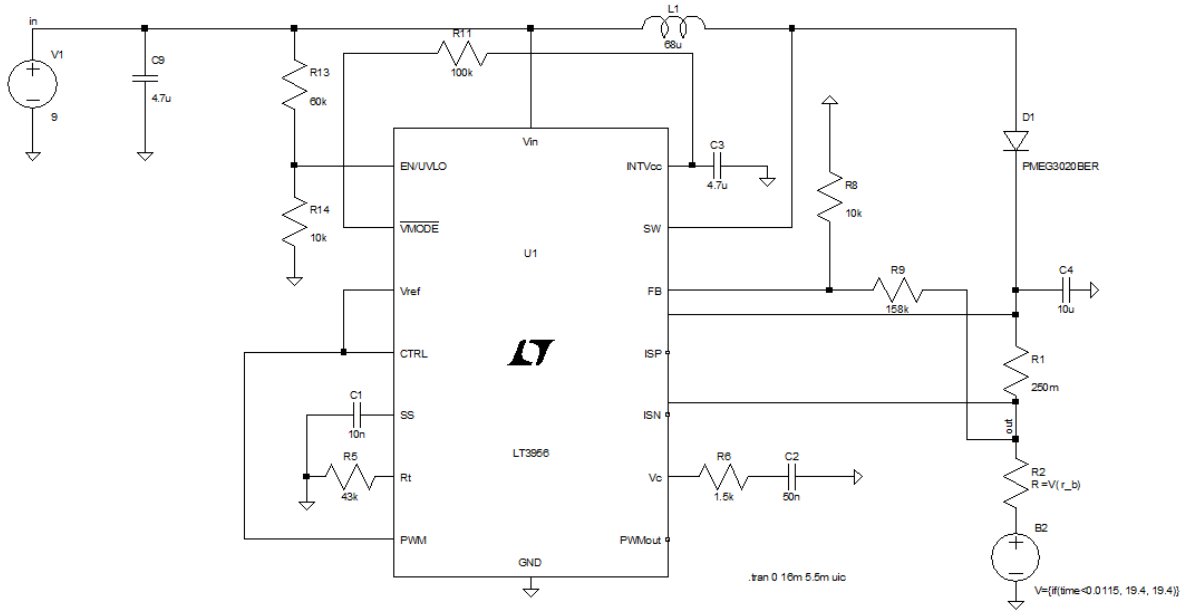

Figure E.4: LTspice simulation setup of the charging circuit.

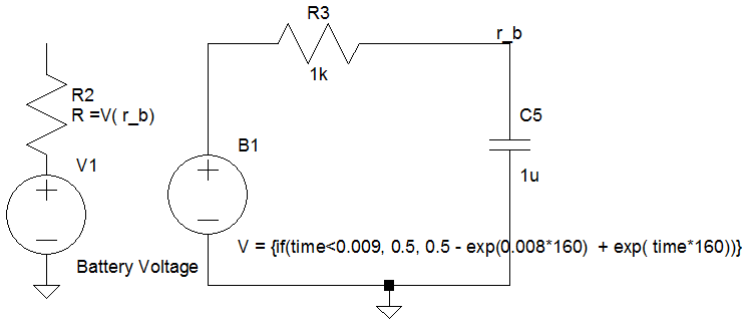

Figure E.5: LTspice setup for the battery model.

E.5. Simulink cell balancing control

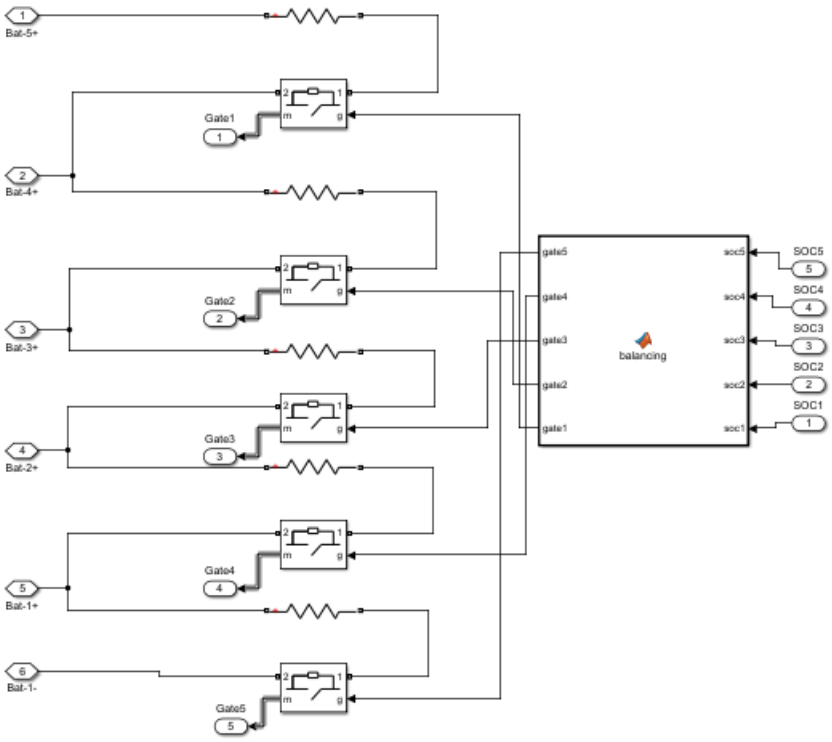

Figure E.6: Simulink setup of the balancing control.

E.6. Simulink battery protection control

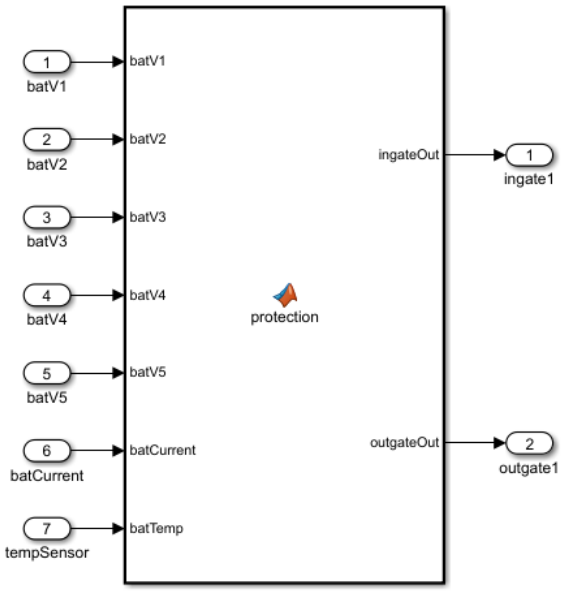

Figure E.7: Simulink setup of the protection control.

E.7. BQ40Z80 Top-level

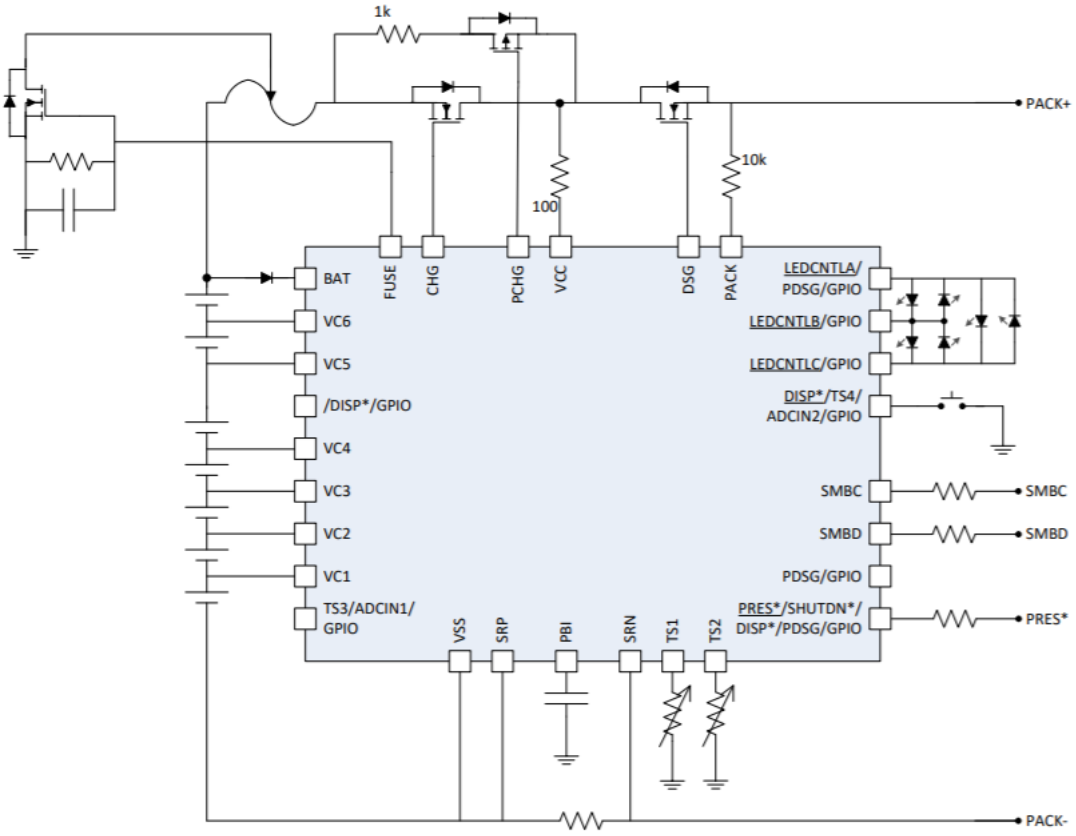

Figure E.8: Simplified schematic of the BQ40Z80 [65].

E.8. BQ40Z80 Cell balancing

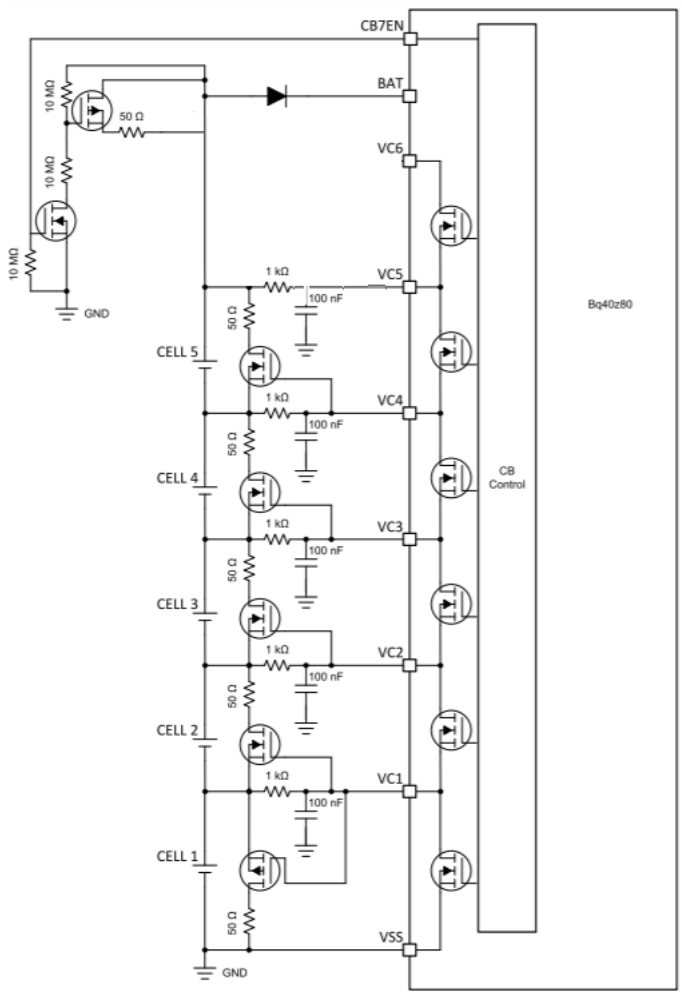

Figure E.9: Cell balancing of the BQ40Z80 for 5 series cells [65].

F

Test Procedure

F.1. CC-mode

Purpose	Verify the working of the CC-mode of the charger.
Requirements	The charger will be in CC-mode when the EN/UVLO pin is above 1.2 V and the FB pin is below 1.25 V.
Procedure	1) Connect a load with 17.5 Ω with its positive terminal to TP3 and negative terminal to TP4. 2) Connect a power supply with positive 9 V to TP1 and negative terminal to TP2. 3) Measure the operation mode on TP5. 4) Measure the load current on TP3.

F.2. CV-mode

Purpose	Verify the working of the CV-mode of the charger.
Requirements	The charger will be in CV-mode when the EN/UVLO pin is above 1.2 V and the FB pin is equal to or above 1.25 V.
Procedure	1) Connect a load with 24.5 Ω with its positive terminal to TP3 and negative terminal to TP4. 2) Connect a power supply with positive 9 V to TP1 and negative terminal to TP2. 3) Measure the operation mode on TP5. 4) Measure the load voltage over TP3 and TP4.

F.3. Mode switching

Purpose	Verify the working of the switching between CC-mode and CV-mode of the charger.
Requirements	The charger will switch from CC-mode to CV-mode when the EN/UVLO pin is above 1.2 V, and the FB pin is increased from below to above 1.25 V.
Procedure	1) Connect a load with 17.5 Ω positive terminal to TP3 and negative terminal to TP4. 2) Connect an output power supply with 18 V and 1.5 A in parallel with the load. 3) Connect an input power supply with positive 9 V to TP1 and negative terminal to TP2. 4) Increase the output power supply from 18 V to 22 V. 5) Measure the operation mode on TP5. 6) Measure the load voltage over TP3 and TP4.

F.4. Inductor current ripple

Purpose	Verify that the inductor current ripple is ≤816.6 mA.
Requirements	Measured both during CC-mode and CV-mode.
Procedure	1) Connect a load with 17.5 Ω (CC) or 24.5 Ω (CV) with its positive terminal to TP3 and negative terminal to TP4. 2) Connect a power supply with positive 9 V to TP1 and negative terminal to TP2. 3) Measure the source current ripple through TP1.

F.5. Output voltage ripple

Purpose	Verify that the output voltage ripple is ≤1.25 V.
Requirements	Measured both during CC-mode and CV-mode.
Procedure	1) Connect a load with 17.5 Ω (CC) or 24.5 Ω (CV) with its positive terminal to TP3 and negative terminal to TP4. 2) Connect a power supply with positive 9 V to TP1 and negative terminal to TP2. 3) Measure the load voltage ripple over TP3 and TP4.

F.6. Output current ripple

Purpose	Verify that the output current ripple is ≤350 mA.
Requirements	Measured during CV-mode.
Procedure	1) Connect a load with 24.5 Ω with its positive terminal to TP3 and negative terminal to TP4. 2) Connect a power supply with positive 9 V to TP1 and negative terminal to TP2. 3) Measure the load voltage ripple over TP3 and TP4.

F.7. Thermal performance

Purpose	Verify the thermal performance of the charger.
Requirements	Measured both during CC-mode and CV-mode.
Procedure	1) Connect a load with 17.5 Ω (CC) or 24.5 Ω (CV) with its positive terminal to TP3 and negative terminal to TP4. 2) Connect a power supply with positive 9 V to TP1 and negative terminal to TP2. 3) Measure the temperature of the following components: a) Schottky diode (D1) b) LT3956 IC (IC1) c) Inductor (L1)

F.8. Efficiency

Purpose	Verify the efficiency of the charger.
Requirements	Measured both during CC-mode and CV-mode.
Procedure	1) Connect a load with 17.5 Ω (CC) or 24.5 Ω (CV) with its positive terminal to TP3 and negative terminal to TP4. 2) Connect a power supply with positive 9 V to TP1 and negative terminal to TP2. 3) Measure the load voltage over TP3 and TP4. 4) Measure the load current through TP3. 5) Measure the source voltage over TP1 and TP2. 6) Measure the source current through TP1.

Bibliography

[1] Charlotte De Jonghe and Gijs Lagerweij. UV-C Sterilizer for the Wireless Powerlizer, 2021. Bachelor Thesis, Delft University of Technology.

[2] Brecht Hurkmans and Floris van der Kolk. Wireless Charging for the Wireless Powerlizer, 2021. Bachelor Thesis, Delft University of Technology.

[3] Dima Kilani, Baker Mohammad, Mohammad Alhawari, Hani Saleh, and Mohammed Ismail. *Power Management for Wearable Electronic Devices*. 01 2020. ISBN 978-3-030-37883-7. doi:10.1007/978-3-030-37884-4.

[4] Plett GL. *Battery Management Systems*. Norwood: Artech House, 2015. ISBN 978-1-630-81024-5. URL https://tudelft.on.worldcat.org/search?queryString=battery#/oclc/978618037.

[5] Yeru Liang, Chen-Zi Zhao, Hong Yuan, Yuan Chen, Weicai Zhang, Jia-Qi Huang, Dingshan Yu, Yingliang Liu, Maria-Magdalena Titirici, Yu-Lun Chueh, Haijun Yu, and Qiang Zhang. A review of rechargeable batteries for portable electronic devices. *InfoMat*, 1(1):6–32, 2019. doi:https://doi.org/10.1002/inf2.12000. URL https://onlinelibrary.wiley.com/doi/abs/10.1002/inf2.12000.

[6] Slobodan Petrovic. *Battery Technology Crash Course: A Concise Introduction*. Springer, 2021. ISBN 978-3-030-57269-3. doi:10.1007/978-3-030-57269-3. URL https://tudelft.on.worldcat.org/search?queryString=battery#/oclc/1202758685.

[7] John T. Warner. Chapter 3 – Lithium-ion battery operation. In John T. Warner, editor, *Lithium-Ion Battery Chemistries*, pages 43–77. Elsevier, 2019. ISBN 978-0-12-814778-8. doi:10.1016/B978-0-12-814778-8.00003-X. URL https://www.sciencedirect.com/science/article/pii/B978012814778800003X.

[8] Xuning Feng, Minggao Ouyang, Xiang Liu, Languang Lu, Yong Xia, and Xiangming He. Thermal runaway mechanism of lithium ion battery for electric vehicles: A review. *Energy Storage Materials*, 10:246–267, 2018. ISSN 2405-8297. doi:10.1016/j.ensm.2017.05.013. URL https://www.sciencedirect.com/science/article/pii/S2405829716303464.

[9] Christopher D. Rahn and Chao-Yang Wang. *Battery Systems Engineering*. John Wiley & Sons, 2013. ISBN 978-1-119-97950-0. URL https://app.knovel.com/hotlink/toc/id:kpBSE0001P/battery-systems-engineering/battery-systems-engineering.

[10] H. Keshan, J. Thornburg, and T. S. Ustun. Comparison of lead-acid and lithium ion batteries for stationary storage in off-grid energy systems. In *4th IET Clean Energy and Technology Conference (CEAT 2016)*, pages 1–7, 2016. doi:10.1049/cp.2016.1287.

[11] Yeru Liang, Chen-Zi Zhao, Hong Yuan, Yuan Chen, Weicai Zhang, Jia-Qi Huang, Dingshan Yu, Yingliang Liu, Maria-Magdalena Titirici, Yu-Lun Chueh, Haijun Yu, and Qiang Zhang. A review of rechargeable batteries for portable electronic devices. *InfoMat*, 1(1):6–32, 2019. doi:10.1002/inf2.12000. URL https://onlinelibrary.wiley.com/doi/abs/10.1002/inf2.12000.

[12] *Sealed Lead-Acid Batteries Technical Manual*. Powersonic, June 2010. URL https://web.archive.org/web/20141212091807/http://www.power-sonic.com/images/powersonic/technical/1277751263_20100627-TechManual-Lo.pdf.

[13] *Ni-MH Handbook For Professionals*. Panasonic, June 2017. URL https://eu.industrial.panasonic.com/sites/default/pidseu/files/downloads/files/panasonic_ni-mh_batteries_handbook_interactive_14_06_17.pdf.

[14] Wenhua Zhu, Ying Zhu, Zenda Davis, and Bruce Tatarchuk. Energy efficiency and capacity retention of Ni–MH batteries for storage applications. *Applied Energy*, 106:307–313, 06 2013. doi:10.1016/j.apenergy.2012.12.025.

[15] K. Young, C. Fierro, and M.A. Fetcenko. Status of Ni/MH battery research and industry. In *2011 IEEE Power and Energy Society General Meeting*, pages 1–3, 2011. doi:10.1109/PES.2011.6039071.

[16] John T. Warner. Chapter 4 – Overview and comparison of different lithium-ion chemistries. In John T. Warner, editor, *Lithium-Ion Battery Chemistries*, pages 79–97. Elsevier, 2019. ISBN 978-0-12-814778-8. doi:10.1016/B978-0-12-814778-8.00004-1. URL https://www.sciencedirect.com/science/article/pii/B9780128147788000041.

[17] L.O. Valøen and M.I. Shoesmith. The effect of PHEV and HEV duty cycles on battery and battery pack performance. In *2007 Plug-in Highway Electric Vehicle Conference*, 2007. URL https://web.archive.org/web/20090326150713/http://www.pluginhighway.ca/PHEV2007/proceedings/PluginHwy_PHEV2007_PaperReviewed_Valoen.pdf.

[18] USB Type-C Spec R2.0 - August 2019. Universal Serial Bus Type-C Cable and Connector Specification. Standard, USB 3.0 Promoter Group, aug 2019.

[19] USB 2.0. Universal Serial Bus Specification. Standard, USB 2.0 Promoter Group, apr 2000.

[20] Battery Charging Specification. Battery Charging Specification. Standard, USB Battery Charging Working Group, mar 2012.

[21] USB 3.2 Revision 1.0. Universal Serial Bus 3.2 Specification. Standard, USB 3.0 Promoter Group, sep 2017.

[22] USB Power Delivery WG Chair. Universal Serial Bus Power Delivery Specification. Standard, USB 3.0 Promoter Group, aug 2019.

[23] Jan Axelson. *USB Complete: The Developer's Guide*. Lakeview Research, 4th edition, 2009. ISBN 1931448086.

[24] *Ansmann 2347-3008-20-520 battery*. Ansmann, January 2020. URL https://docs.rs-online.com/907a/A700000007373973.pdf. Version 4.

[25] Joao Figueiredo, Fernando Tofoli, and Ricardo Alves. Comparison of nonisolated dc-dc converters from the efficiency point of view. pages 14–19, 09 2011. ISBN 978-1-4577-1644-7. doi:10.1109/COBEP.2011.6085174.

[26] Mark Harris. USB Power Delivery for Your Next Project, 2020. URL https://resources.altium.com/p/usb-power-delivery-your-next-project. [Accessed: 19.05.2021].

[27] *STM32L562xx*. STMicroelectronics, September 2020. URL https://www.st.com/resource/en/datasheet/stm32l562re.pdf. Rev. 4.

[28] *STM32 Cortex®-M33 MCUs programming manual*. STMicroelectronics, February 2020. URL https://www.st.com/resource/en/programming_manual/dm00650283-stm32-cortexm33-mcus-programming-manual-stmicroelectronics.pdf. Rev. 1.

[29] Bita Arabsalmanabadi, Nima Tashakor, Alireza Javadi, and Kamal Al-Haddad. Charging Techniques in Lithium-Ion Battery Charger: Review and New Solution. In *IECON 2018 - 44th Annual Conference of the IEEE Industrial Electronics Society*, pages 5731–5738, 2018. doi:10.1109/IECON.2018.8591173.

[30] Jiuyu Du and Yizhao Sun. The Influence of High Power Charging on the Lithium Battery Based on Constant and Pulse Current Charging Strategies. In *2020 IEEE Vehicle Power and Propulsion Conference (VPPC)*, pages 1–7, 2020. doi:10.1109/VPPC49601.2020.9330884.

[31] L Rao, Sanjay Gairola, Sandhya Lavety, and Noorul Islam. Design of DC-DC Boost Converter with Negative Feedback Control for Constant Current Operation. *International Journal of Power Electronics and Drive Systems (IJPEDS)*, 8:1575, 12 2017. doi:10.11591/ijpeds.v8.i4.pp1575-1584.

[32] How to Design a Simple Constant Current/Constant Voltage Buck Converter. Technical report, Texas Instruments, June 2018. URL https://www.ti.com/lit/an/snva829/snva829.pdf.

[33] Alexander Bubovich. The comparison of different types of DC-DC converters in terms of low-voltage implementation. In *2017 5th IEEE Workshop on Advances in Information, Electronic and Electrical Engineering (AIEEE)*, pages 1–4, 2017. doi:10.1109/AIEEE.2017.8270560.

[34] Sven De Breucker, Kristof Engelen, Reinhilde D'hulst, and Johan Driesen. Impact of current ripple on Li-ion battery ageing. *2013 World Electric Vehicle Symposium and Exhibition, EVS 2014*, 6, 10 2014. doi:10.1109/EVS.2013.6914791.

[35] Basic Calculation of a Boost Converter's Power Stage (Rev. C). Technical report, Texas Instruments, 2014. URL https://www.ti.com/lit/an/slva372c/slva372c.pdf.

[36] Loizos Efthymiou, Gianluca Camuso, Giorgia Longobardi, Florin Udrea, Evelyn Lin, Terry Chien, and Max Chen. Zero reverse recovery in SiC and GaN Schottky diodes: A comparison. In *2016 28th International Symposium on Power Semiconductor Devices and ICs (ISPSD)*, pages 71–74, 2016. doi:10.1109/ISPSD.2016.7520780.

[37] Soo Seok Choi and Hong S Lim. Factors that affect cycle-life and possible degradation mechanisms of a Li-ion cell based on LiCoO2. *Journal of Power Sources*, 111(1):130–136, 2002. ISSN 0378-7753. doi:10.1016/S0378-7753(02)00305-1. URL https://www.sciencedirect.com/science/article/pii/S0378775302003051.

[38] *MPXV1D1250L680 68uH 4.5A Shielded Power Inductor*. KEMET, 2021. URL https://api.kemet.com/component-edge/download/specsheet/MPXV1D1250L680.pdf.

[39] *MPXV1D2213L680 68uH 12.5A Shielded Power Inductor*. KEMET, 2021. URL https://api.kemet.com/component-edge/download/specsheet/MPXV1D2213L680.pdf.

[40] *AVX 12065D106KAT2A datasheet*. AVX, August 2018. URL https://spicat.avx.com/product/mlcc/chartview/12065D106KAT2A/DataSheet/X5R.

[41] *LT3956 Constant-Current, Constant-Voltage Converter*. Linear Technology, May 2010. URL https://www.analog.com/media/en/technical-documentation/data-sheets/3956f.pdf.

[42] *PMEG3020BER datasheet*. Nexperia, February 2018. URL https://assets.nexperia.com/documents/data-sheet/PMEG3020BER.pdf.

[43] MathWorks. Generic battery model – Simulink, 2020. URL https://nl.mathworks.com/help/physmod/sps/powersys/ref/battery.html. [Accessed: 24.05.2021].

[44] Fei Zhang, Guangjun Liu, and Lijin Fang. A battery State of Charge estimation method with extended Kalman filter. In *2008 IEEE/ASME International Conference on Advanced Intelligent Mechatronics*, pages 1008–1013, 2008. doi:10.1109/AIM.2008.4601799.

[45] Youngbin Song, Minjun Park, Minhwan Seo, and Sang Woo Kim. Improved SOC estimation of lithium-ion batteries with novel SOC-OCV curve estimation method using equivalent circuit model. In *2019 4th International Conference on Smart and Sustainable Technologies (SpliTech)*, pages 1–6, 2019. doi:10.23919/SpliTech.2019.8783149.

[46] Mehdi Gholizadeh, Alireza Yazdizadeh, Mohsen Rahmati, and Abbas Aliabadi. SOC estimation for a lithium-ion battery by designing a nonlinear observer based on an equivalent circuit model. In *2017 IEEE 15th International Conference on Industrial Informatics (INDIN)*, pages 628–632, 2017. doi:10.1109/INDIN.2017.8104844.

[47] A.G. Stefanopoulou and Y. Kim. 10 - System-level management of rechargeable lithium-ion batteries. In Alejandro A. Franco, editor, *Rechargeable Lithium Batteries*, Woodhead Publishing Series in Energy, pages 281–302. Woodhead Publishing, 2015. ISBN 978-1-78242-090-3. doi:https://doi.org/10.1016/B978-1-78242-090-3.00010-9. URL https://www.sciencedirect.com/science/article/pii/B9781782420903000109.

[48] Rui Xiong. *Battery management algorithm for electric vehicles*. Springer, 2020. doi:10.1007/978-981-15-0248-4. URL https://tudelft.on.worldcat.org/oclc/1121267494.

[49] D. Satou. Real-time Battery Cell Voltage Measurement Method Using LC Series Circuit Type Cell Voltage Equalizer. In *2019 IEEE 4th International Future Energy Electronics Conference (IFEEC)*, pages 1–4, 2019. doi:10.1109/IFEEC47410.2019.9015080.

[50] L. Wei, L. Jie, S. Wenji, and F. Ziping. Study on passive balancing characteristics of serially connected lithium-ion battery string. In *2017 13th IEEE International Conference on Electronic Measurement Instruments (ICEMI)*, pages 489–495, 2017. doi:10.1109/ICEMI.2017.8265862.

[51] O. F. GOKSU and R. ACAR VURAL. Battery Management Module with Active Balancing and Cell Switching. In *2018 6th International Conference on Control Engineering Information Technology (CEIT)*, pages 1–6, 2018. doi:10.1109/CEIT.2018.8751773.

[52] Mohamed Daowd, Noshin Omar, Peter Van Den Bossche, and Joeri Van Mierlo. Passive and active battery balancing comparison based on MATLAB simulation. In *2011 IEEE Vehicle Power and Propulsion Conference*, pages 1–7, 2011. doi:10.1109/VPPC.2011.6043010.

[53] Neil Samaddar, Senthil Kumar, and R. Jayapragash. Passive Cell Balancing of Li-Ion batteries used for Automotive Applications. *Journal of Physics: Conference Series*, 1716:012005, 12 2020. doi:10.1088/1742-6596/1716/1/012005.

[54] Kyung-Min Lee, Yoo-Chae Chung, Chang-Hyeon Sung, and Bongkoo Kang. Active Cell Balancing of Li-Ion Batteries Using LC Series Resonant Circuit. *IEEE Transactions on Industrial Electronics*, 62(9):5491–5501, 2015. doi:10.1109/TIE.2015.2408573.

[55] Chao Wu, Jinlei Sun, Chunbo Zhu, Yunwang Ge, and Yongping Zhao. Research on Overcharge and Overdischarge Effect on Lithium-Ion Batteries. In *2015 IEEE Vehicle Power and Propulsion Conference (VPPC)*, pages 1–6, 2015. doi:10.1109/VPPC.2015.7353006.

[56] Masahiro Ichimura. The safety characteristics of lithium-ion batteries for mobile phones and the nail penetration test. In *INTELEC 07 - 29th International Telecommunications Energy Conference*, pages 687–692, 2007. doi:10.1109/INTLEC.2007.4448869.

[57] R. Guo, L. Lu, and M. Ouyang. Mechanism of the entire overdischarge process and overdischarge-induced internal short circuit in lithium-ion batteries. In *Scientific Reports*, volume 6, 2016. doi:10.1038/srep30248.

[58] Seunghyeong Lee, Yongjae Jeong, Yungwi Song, and Jongsun Kim. A single chip Li-Ion battery protection IC with low standby mode auto release. In *2014 International SoC Design Conference (ISOCC)*, pages 38–39, 2014. doi:10.1109/ISOCC.2014.7087583.

[59] Hongwei Wang, Defu Xia, Nianpeng Si, Ziqiang Tao, Yanling Fu, Haiqing Xiao, Hua Bai, and Shuang Dena. Impact of Ambient Temperature on the Consistency of Lithium ion Batteries. In *2018 International Conference on Sensing,Diagnostics, Prognostics, and Control (SDPC)*, pages 763–766, 2018. doi:10.1109/SDPC.2018.8664960.

[60] R. Srinivasan, P. Demirev, B. Carkhuff, Santhanagopalan S., J. Jeevarajan, and T. Barrera. Review – Thermal Safety Management in Li-Ion Batteries: Current Issues and Perspectives. In *Journal of the Electrochemical Society*, volume 167, 2020. doi:10.1149/1945-7111/abc0a5.

[61] Aaron Knobloch, Jason Karp, Yuri Plotnikov, Chris Kapusta, Jason Siegel, Nassim Samad, and Anna Stefanopoulou. Novel thin temperature and expansion sensors for li-ion battery monitoring. In *2017 IEEE SENSORS*, pages 1–3, 2017. doi:10.1109/ICSENS.2017.8234066.

[62] *LTC3300-1 High Efficiency Bidirectional Multicell Battery Balancer*. Analog Devices, June 2019. URL https://www.analog.com/media/en/technical-documentation/data-sheets/LTC3300-1.pdf. Rev. C.

[63] *LTC3300-2 Addressable High Efficiency Bidirectional Multicell Battery Balancer*. Analog Devices, May 2019. URL https://www.analog.com/media/en/technical-documentation/data-sheets/LTC3300-2.pdf. Rev. B.

[64] *BQ40Z80 2-Series to 6-Series Li-Ion Battery Pack Manager*. Texas Instruments, June 2018. URL https://www.ti.com/lit/ds/symlink/bq40z80.pdf?ts=1622682025114&ref_url=https%253A%252F%252Fwww.ti.com%252Fproduct%252FBQ40Z80. Rev. B.

[65] *BQ40Z80 Technical Reference*. Texas Instruments, October 2019. URL https://www.ti.com/lit/ug/sluubt5b/sluubt5b.pdf?ts=1622696167688&ref_url=https%253A%252F%252Fwww.ti.com%252Fproduct%252FBQ40Z80. Rev. B.